iScience

CellPress
OPEN ACCESS

Article

Culin5 aggravates hypoxic pulmonary hypertension by activating TRAF6/NF-κB/HIF-1α/VEGF

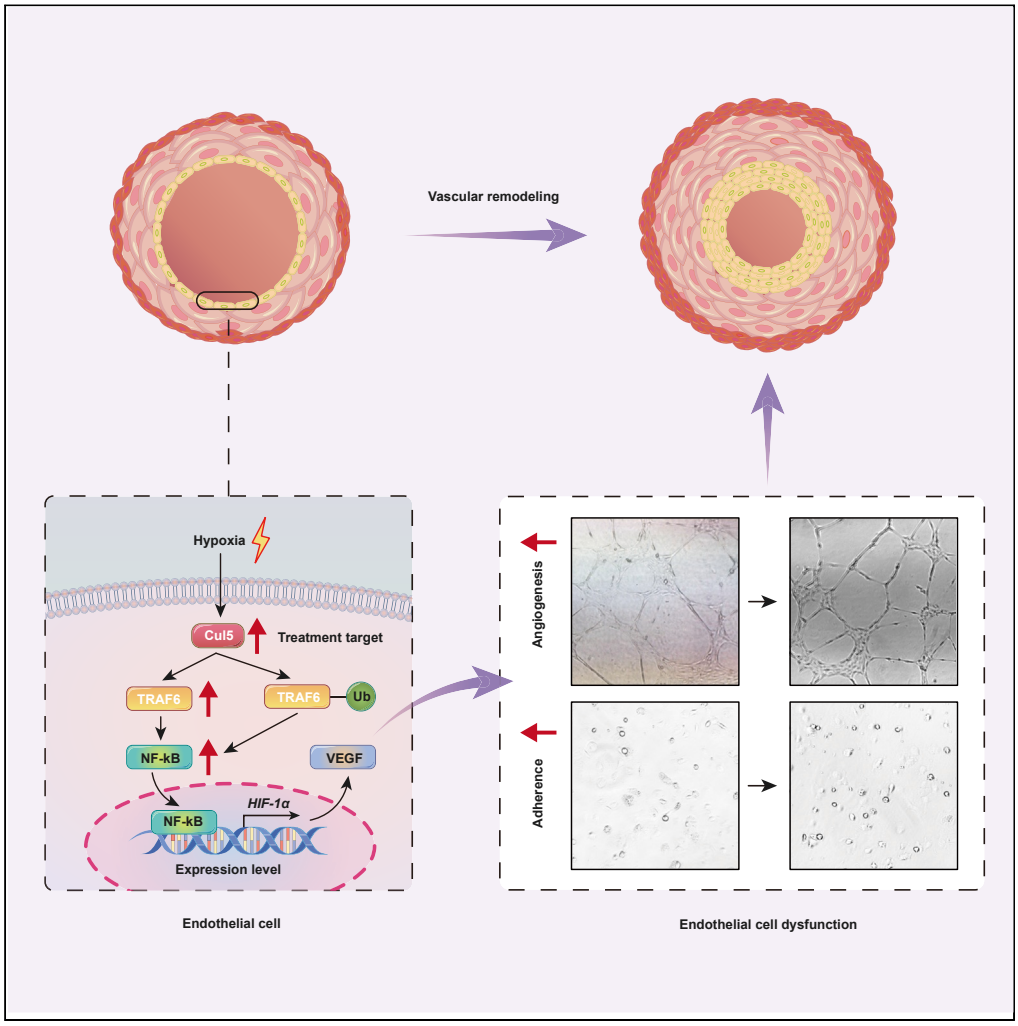

Lei Wang, Jing Huang, Ruoyang Zhang, ..., Sun Ying, Jie Liu, Chen Wang

liujie@ccmu.edu.cn

Highlights

Cul 5 participates in the pathogenesis of hypoxic pulmonary vascular remodeling

Cul 5 activates TRAF6/NF-κB/HIF-1α/VEGF signaling

Cul 5/TRAF6/NF-κB/HIF-1α/VEGF signaling is involved in endothelial dysfunction

Targeting Cul 5 could alleviate hypoxic pulmonary vascular remodeling

Wang et al., iScience 26, 108199
November 17, 2023
https://doi.org/10.1016/j.isci.2023.108199

iScience

CellPress
OPEN ACCESS

Article

Culin5 aggravates hypoxic pulmonary hypertension by activating TRAF6/NF-κB/HIF-1α/VEGF

Lei Wang,[1,4] Jing Huang,[2] Ruoyang Zhang,[3,4] Muzhi Zhang,[3,4] Yu Guo,[3,4] Yang Liu,[3,4] Cong Li,[1] Wei Wang,[3,4] Sun Ying,[3,4] Jie Liu,[3,4,5,*] and Chen Wang[4]

SUMMARY

Hypoxic pulmonary hypertension (HPH) lacks effective pharmacologic treatments. Microarray-based gene expression indicates the crucial role of Cullin 5 (Cul 5) in HPH. This study showed that Cul 5 was up-regulated in HPH patients and a murine model of HPH. *In vitro*, Cul 5 promoted the angiogenesis and adhesion capacity of human pulmonary artery endothelial cells (PAECs), which could be mitigated by Cul 5 inactivation mediated by pevonedistat or NEDD8 silence. *In vivo*, silencing of Cul 5 in the endothelium and Cul 5 inactivation by pevonedistat could also alleviate hypoxic vascular remodeling. Mechanistic research showed that Cul 5 participated in HPH pathogenesis via the TRAF6/NF-κB/HIF-1α/VEGF pathway. Inhibition of the TRAF6/NF-κB/HIF-1α/VEGF pathway could reverse Cul 5-induced human PAEC dysfunction. These findings demonstrate that Cul 5 is an important mediator of HPH via the TRAF6/NF-κB/HIF-1α/VEGF pathway firstly, and could be considered as a potential therapeutic target in the clinical treatment of HPH.

INTRODUCTION

Hypoxic pulmonary hypertension (HPH) is a subset of 5 types of pulmonary hypertension (PH) due to lung diseases and/or hypoxia,[1] and is characterized by persistent elevation of pulmonary arterial pressure and vascular remodeling. Hypoxia initially induces acute pulmonary vasoconstriction, and then vascular remodeling, which participate in the development of HPH. Pulmonary vascular remodeling is the key structural alteration in HPH, and involves changes in the intima, media, and adventitia.[2]

Endothelial dysfunction plays a major role in the initiation of pulmonary vascular remodeling and is thought to be a major contributor to this process.[3] Currently, none of the available therapeutic modalities in the clinic have shown the potential to prevent and reverse pulmonary vascular remodeling, which results from an incomplete understanding of the signaling pathways that drive endothelial dysfunction. Some basic studies have shown that improving endothelial function could reverse pulmonary vascular remodeling,[4,5] so it is important to clarify endothelial injury mechanisms for PH treatment, especially hypoxia-induced endothelial injury. The vascular endothelial growth factor (VEGF) pathway is a master regulator of angiogenesis and a crucial regulator of vascular development,[6] and it has been proven that the VEGF pathway of endothelial cells isolated from PH patients is hyperactivated.[7,8] We have proved that IL33 induced HIF-1α/VEGF activation played an important role in the hypoxia-induced pulmonary vascular remodeling,[9] while the VEGF pathway activation mechanism in HPH need to be clarified further.

Our microarray analysis indicated that Cullin 5 (Cul 5) is upregulated in human pulmonary artery endothelial cells (PAECs) under hypoxia and has the highest degree in the differentially expressed gene interaction network. Cul 5 proteins are expressed in various organs and many types of cells of the immune system, especially in the lungs; however, the function of Cul 5 in respiratory disease remains poorly understood. It has been reported that Cul 5 is expressed in cultured rat endothelial cells,[10] which is an important element in cardiovascular biology.[11] At present, the role of Cul 5 in vascular diseases, especially PH, is under clarification. In a previous study, we have proved that HIF-1α/VEGF promotes HPH progression,[9] and it was reported that Cul-5 and TRAF6 interaction could lead to NF-κB activation,[12] which is an important direct modulator of HIF-1α expression.[13] Up to now, whether Cul 5 is involved in VEGF pathway activation via TRAF6/NF-κB/HIF-1α during HPH pathogenesis is also unknown.

This study aimed to clarify the role of Cul-5 in pulmonary vascular remodeling during HPH development and its role in VEGF pathway activation. This mechanism may provide a potential role for Cul-5 in HPH therapeutic applications.

[1]Department of Respiratory and Critical Care Medicine, The Second Affiliated Hospital of Xi'an Jiaotong University (Xibei Hospital), Xi'an, Shaanxi 710004, China
[2]Department of Rheumatism and Immunology, The First Affiliated Hospital Xi'an Jiaotong University, Xi'an, Shaanxi 710061, China
[3]Department of Immunology, School of Basic Medical Sciences, Capital Medical University, Beijing 100054, China
[4]Department of Respiratory Medicine, Capital Medical University, Beijing 100054, P.R. China
[5]Lead contact
*Correspondence: liujie@ccmu.edu.cn
https://doi.org/10.1016/j.isci.2023.108199

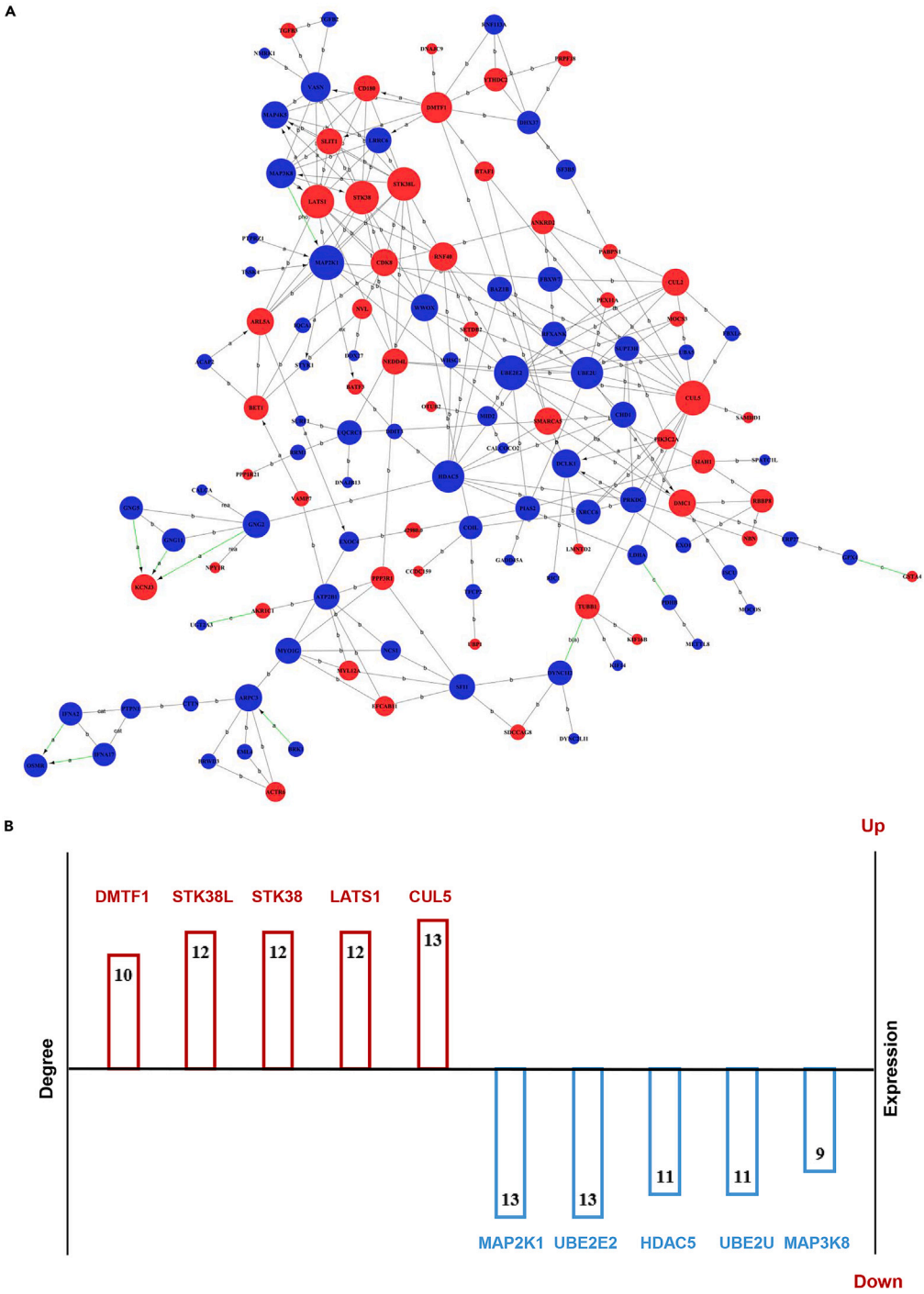

Figure 1. Crucial role of Cul 5 in the hypoxia-induced endothelial cell injury recognized by silico analysis

(A) Global Signal Transduction Network of differentially expressed mRNAs. This network shows the gene-gene functional interaction, a node represents a gene, red color indicates upregulation and blue color indicates downregulation. The edges connect the nodes represents the relationships between them. The indicators a, b, cat, c, ex, pho, and r are abbreviation of activation, binding, catalysis, compound, expression, phosphorylation, and reaction, respectively.

(B) The top 10 genes of high value of degree. The degree represents the number of directly linked genes within the network.

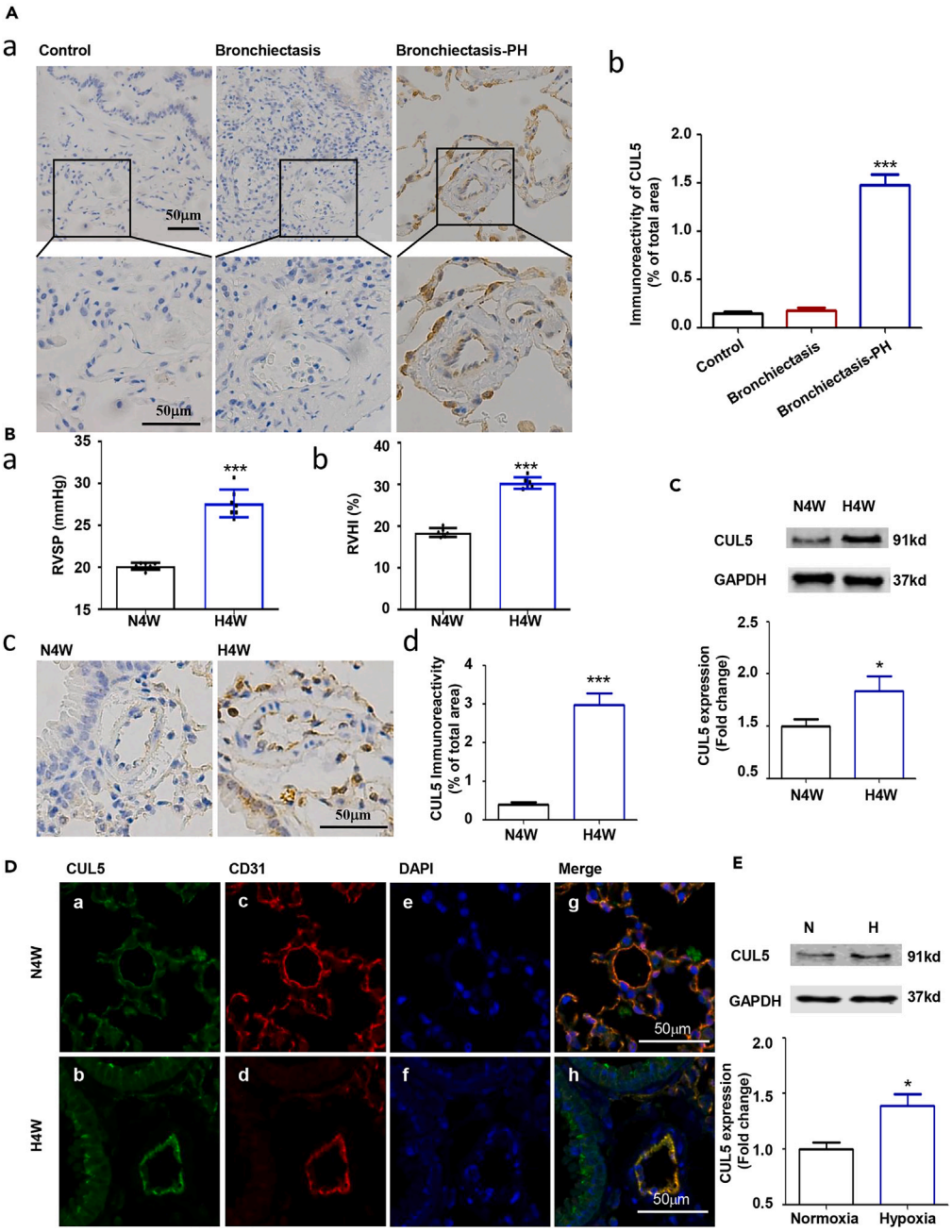

Figure 2. Upregulation of Cul 5 in HPH

(A) Increased expression of Cul5 in HPH patients. (a) Immunoreactivity for Cul5 (brown) in lung tissues from patients of bronchiectasis with or without PH and a normal control. Immunoreactivity for Cul5 was located predominantly in the innermost medial layer of pulmonary arterioles. Scale bars: 50 μm. (b) Bar chart for Cul5 staining of lung tissue sections from patients. ***$p < 0.001$ (vs. Control). Data are represented as the means ± SD, one-way ANOVA was used for statistical analysis.

(B) Increased expression of Cul5 in HPH mouse model detected by IHC. (a) RVSP of mice exposed to normoxia (N4W) and hypoxia (H4W) for 4 weeks ***$p < 0.001$. Student's *t* test was used for statistical analysis. (b) RVHI of mice exposed to normoxia (N4W) and hypoxia (H4W) for 4 weeks ***$p < 0.001$. Student's *t* test was used for statistical analysis. (c) Increased expression of Cul5 in mice exposed to normoxia (N4W) or to hypoxia (H4W) for 4 weeks. Immunoreactivity for Cul5 was located predominantly in the innermost medial layer of pulmonary arterioles. Scale bars: 50 μm. (d) Bar chart for Cul5 immunoreactivity signal of lung tissue sections from mice. ***$p < 0.001$. Data are represented as the means ± SD, Student's *t* test was used for statistical analysis.

(C) Increased expression of Cul5 in HPH mouse model detected by WB. *$p < 0.05$. Data are represented as the means ± SD, Student's *t* test was used for statistical analysis.

(D) Upregulated expression of Cul5 measured by immunofluorescent analysis in HPH mouse model. (a and b) tissue sections were immunostained with Cul5; (c and d) tissue sections were immunostained with CD31; (e and f) nuclei were stained with DAPI; (g and h) merged picture. Scale bars: 50 μm.

(E) Increased expression of Cul5 in endothelial cells exposed to hypoxia detected by WB. *$p < 0.05$. Data are represented as the means ± SD, Student's *t* test was used for statistical analysis.

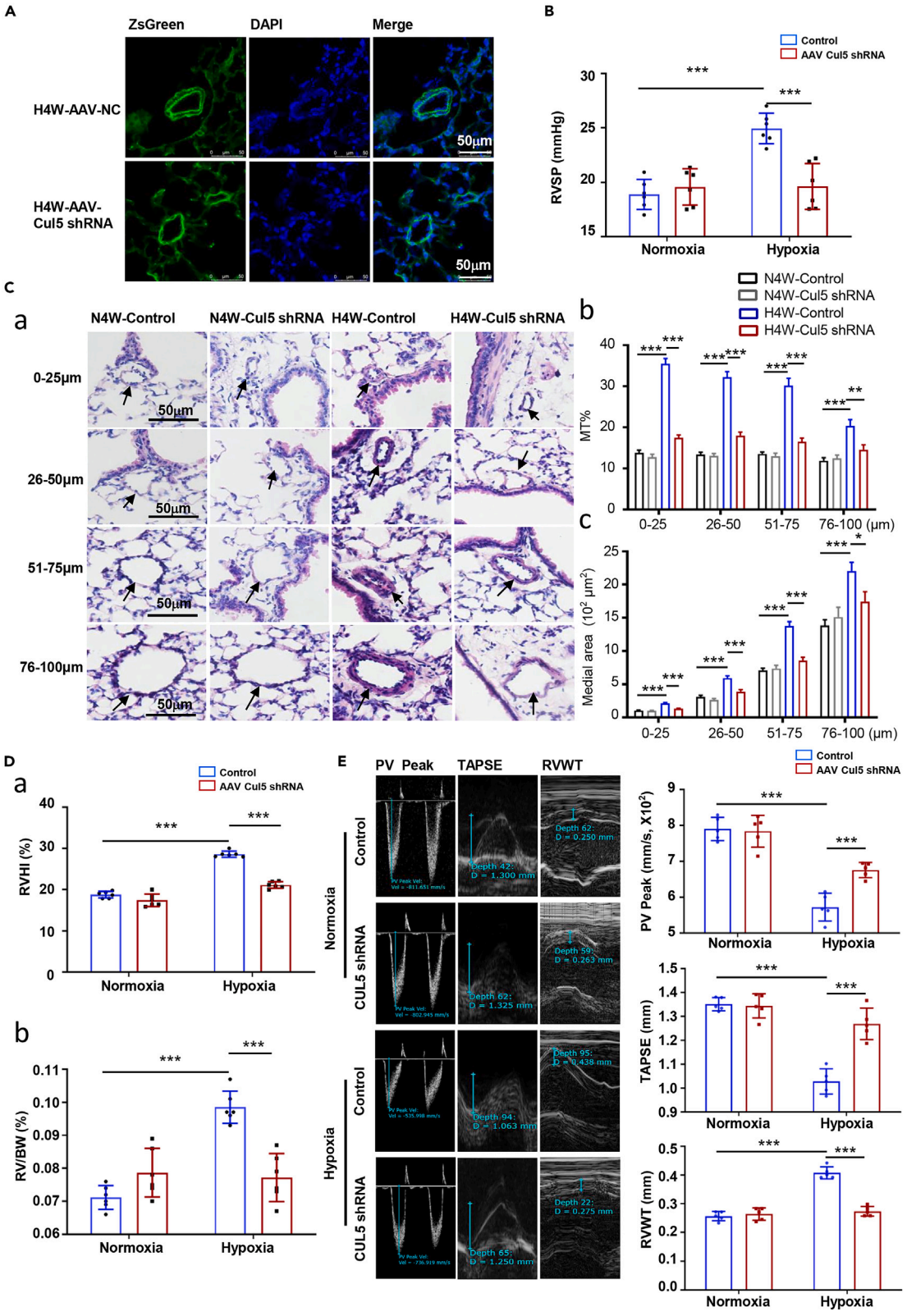
A
ZsGreen
DAPI
Merge
H4W-AAV-NC
H4W-AAV-Cul5 shRNA
50μm
B
Control
AAV Cul5 shRNA
RVSP (mmHg)
Normoxia
Hypoxia
C
a
N4W-Control
N4W-Cul5 shRNA
H4W-Control
H4W-Cul5 shRNA
0-25μm
26-50μm
51-75μm
76-100μm
b
MT%
c
Medial area (10² μm²)
0-25
26-50
51-75
76-100 (μm)
D
a
RVHI (%)
b
RV/BW (%)
E
PV Peak
TAPSE
RVWT
Normoxia
Hypoxia
Control
CUL5 shRNA
PV Peak (mm/s, X10²)
TAPSE (mm)
RVWT (mm)

Figure 3. Alleviation effect of Cul 5 silence on HPH mediated by AAV Cul 5 shRNA

(A) Immunofluorescence staining of ZsGreen (green) in the endothelium of lung tissues, showing the successful transfection of AAV vector. Scale bars: 50 μm.

(B) RVSP of mice from four groups, normoxia-control, normoxia-AAV Cul5 shRNA, hypoxia-control, and hypoxia-AAV Cul5 shRNA. ***$p < 0.001$.

(C) (a) Comparison of pulmonary vascular remodeling of different external diameter pulmonary arterioles (0–25 μm, 26–50 μm, 51–75 μm, and 76–100 μm) among groups. Scale bars: 50 μm. (b) %MT of pulmonary arterioles of mice grouped by external diameter; (c) Medial area of pulmonary arterioles of mice grouped by external diameter. *$p < 0.05$, **$p < 0.01$, ***$p < 0.001$.

(D) Right ventricular hypertrophy of the above groups. (a) RVHI of mice; (b) RV/BW ratio of mice. ***$p < 0.001$.

(E) Echocardiography showing the representative figures and statistical analysis of PV Peak, TAPSE, and RVWT. ***$p < 0.001$. Data are represented as the means ± SD, one-way ANOVA was used for statistical analysis in Figure 3.

RESULTS

In silico analysis of microarray-based gene expression indicates the crucial role of Cul 5 in hypoxia-induced endothelial cell injury

To understand how the mRNAs were differentially expressed in PAECs after hypoxia exposure, we employed microarray analysis to identify the differentially expressed RNAs (fold change >1.1, $p < 0.05$). We found 1,216 differentially expressed mRNAs, including 616 upregulated mRNAs and 600 downregulated mRNAs (Figure S1). The functions of the differentially expressed genes were analyzed according to the Gene Ontology (GO) and pathway according to KEGG. GO analysis revealed that the differentially expressed mRNAs were involving in 24 upregulated biological process ($p < 0.01$, Figure S2) and 36 downregulated biological process ($p < 0.01$, Figure S3). Pathway analysis showed that there are 3 upregulated pathways ($p < 0.05$, Figure S4) and 12 downregulated pathways ($p < 0.05$, Figure S5).

The differentially expressed gene interaction relationships were analyzed with the help of the KEGG database. The interaction relationships include activation, binding, catalysis, compound, expression, phosphorylation, and reaction, and the gene interaction network is shown in Figure 1A. Among the 1,216 differentially expressed mRNAs, 147 mRNAs interacted with each other. The top 10 genes with high degree values (the number of directly linked genes within the network) were CUL5, MAP2K1, UBE2E2, LATS1, STK38, STK38L, HDAC5, UBE2U, DMTF1, and MAP3K8 (Figure 1B). Cul 5 was the top upregulated gene, which may play an important role in endothelial dysfunction derived pulmonary vascular remodeling.

Cul 5 is upregulated in the pulmonary endothelium during HPH pathogenesis

First, the expression of Cul 5 in HPH patients was observed, and information on HPH patients can be seen in our previous study[14] and Table S1. As shown in Figure 2A, immunohistochemistry revealed that immunoreactivity for Cul 5 was located predominantly in the innermost medial layer of pulmonary arterioles. Staining was evident in tissue sections from patients with bronchiectasis-induced PH but less evident in sections from bronchiectasis patients or donor lung tissues.

To determine whether the expression of Cul 5 is changed in mice exposed to hypoxia, we established a hypoxia-induced PH (HPH) mouse model by exposing mice to hypoxia for 4 weeks (H4W). Then, we determined the protein expression of Cul 5 in the lung tissues of mice by immunohistochemical staining (Figure 2B) and western blotting (Figure 2C) and found that Cul 5 in the lung tissues of group H4W mice was obviously upregulated compared with N4W group. Then, we examined Cul 5 expression in mouse lung tissue using immunofluorescent analysis. As shown in Figure 2D, Cul 5 was upregulated in remodeling pulmonary arterioles of HPH mice compared with mice under normoxia, and was mainly distributed along the endothelium. *In vitro*, we also observed that Cul 5 was upregulated in PAECs exposed to hypoxia compared with PAECs under normoxic conditions (Figure 2E).

Silencing of Cul5 reverses HPH *in vivo*

To identify the effects of Cul 5 on HPH *in vivo* further, the recombinant HBAAV2/VEC carrying the mouse CUL5 shRNA and negative control were constructed as described previously. Before exposed to hypoxia, the HBAAV2/VEC-Tie-ZsGreen vectors were given and mainly trapped in the endothelium of lung tissues (Figure 3A). Hypoxia-induced right ventricular systolic pressure (RVSP) increase improved by silencing of Cul5 (Figure 3B). As showed in Figure 3C, silencing of Cul5 also alleviated hypoxia induced pulmonary vascular remodeling, especially the <75 μm intra pulmonary arteriole remodeling.

RVHI and right ventricle (RV)/body weight (BW) was increased under hypoxia, which was alleviated by silencing of Cul5 (Figure 3D). In addition, pulmonary valve (PV) peak velocity, tricuspid annular plane systolic excursion (TAPSE) and RV free wall thickness (RVWT) measured by echocardiography (Figure 3E), decrease of PV peak velocity/TAPSE and increase of RVWT were found in the HPH model, which could be reversed by Cul5 silencing.

Inactivating Cul 5 reverses HPH *in vivo*

Protein modification with the ubiquitin-like molecule (Ubl) NEDD8 called protein NEDDylation is emerging as an important regulatory pathway,[15] and the biological function of Cul 5 depends on its NEDD8 modification.[12] All Cullins are subject to neddylation, which involves conjugation of Nedd8 to the carboxy-terminal domain of Cullins, pevonedistat is a small molecule inhibitor of Nedd8-activating enzyme, that specifically inhibits the NEDD8 E1-activating enzyme and then inactive Cul 5. Recent studies have shown that pevonedistat has antitumor activities.[16] As shown in Figures 4A, a, under hypoxia condition, free NEDD8 was downregulated in PAECs, while NEDD8 bound to Cullins

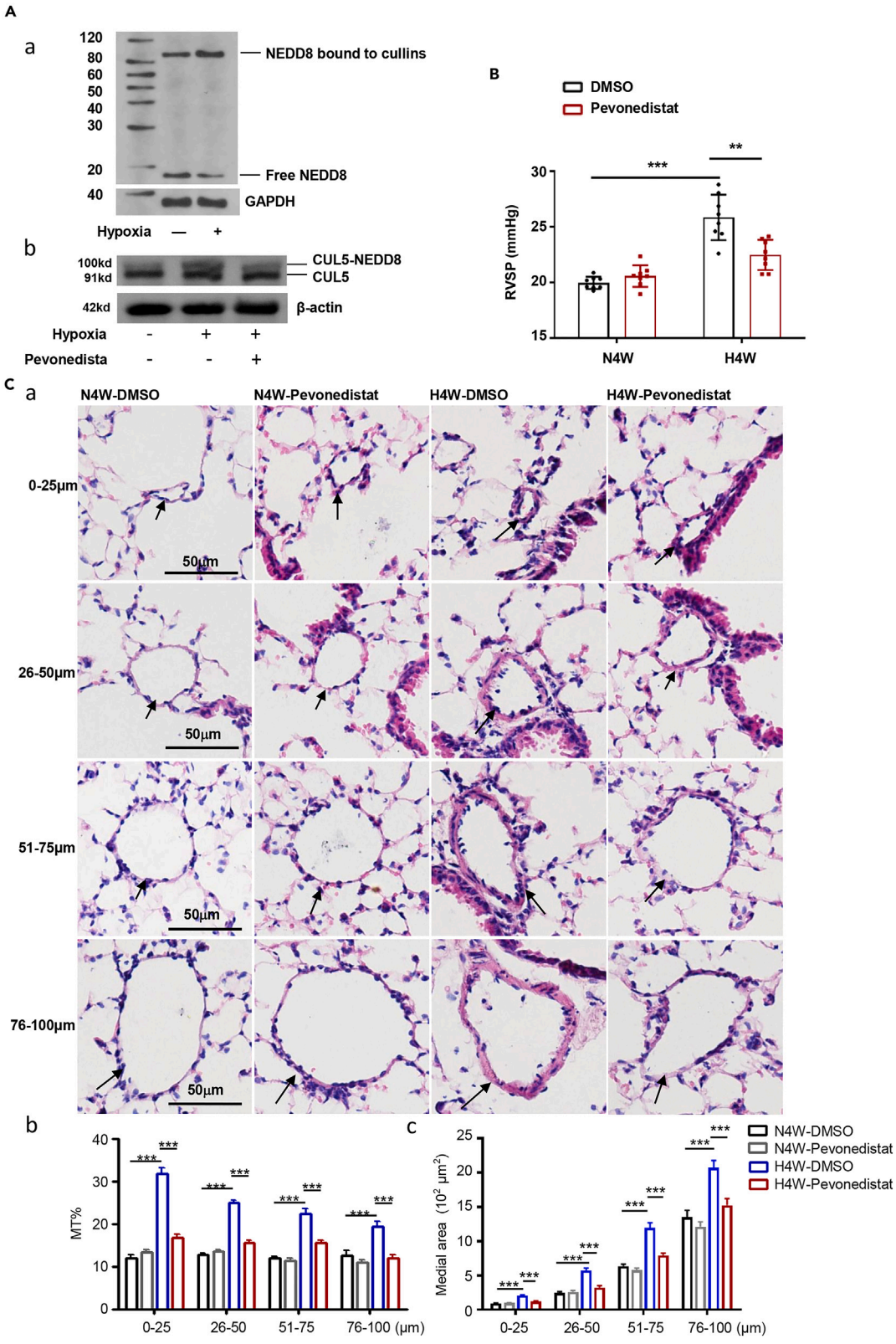
A
a
120
80
60
50
40
30
20
40
NEDD8 bound to cullins
Free NEDD8
GAPDH
Hypoxia — +
b
100kd
91kd
CUL5-NEDD8
CUL5
42kd
β-actin
Hypoxia - + +
Pevonedista - - +
B
DMSO
Pevonedistat
RVSP (mmHg)
30
25
20
15
***
**
N4W
H4W
C
a
N4W-DMSO
N4W-Pevonedistat
H4W-DMSO
H4W-Pevonedistat
0-25μm
26-50μm
51-75μm
76-100μm
50μm
b
MT%
40
30
20
10
0
0-25
26-50
51-75
76-100 (μm)
c
Medial area (10² μm²)
25
20
15
10
5
0
N4W-DMSO
N4W-Pevonedistat
H4W-DMSO
H4W-Pevonedistat

Figure 4. Alleviation effect of Cul 5 inactivator pevonedistat on HPH

(A) Level of Cul 5 NEDDylation. (a) Free NEDD8 and NEDD8 bound to Cullins detected by WB under normoxia and hypoxia; (b) Nedd8 modification of Cul 5 detected by WB under normoxia and hypoxia treated with or without pevonedistat.

(B) RVSP of mice exposed to normoxia (N4W) and hypoxia (H4W) with or without pevonedistat for 4 weeks **p < 0.01, ***p < 0.001.

(C) Comparison of pulmonary vascular remodeling of different external diameter pulmonary arterioles (0–25 μm, 26–50 μm, 51–75 μm, and 76–100 μm) among groups of N4W + DMSO, N4W + pevonedistat, H4W+ DMSO, and H4W + pevonedistat. (a) H&E staining of pulmonary arterioles; Scale bars: 50 μm. (b) %MT of pulmonary arterioles of mice grouped by external diameter; (c) Medial area of pulmonary arterioles of mice grouped by external diameter. ***p < 0.001.Data are represented as the means ± SD, one-way ANOVA was used for statistical analysis in (B and C).

was upregulated. Figures 4A, b also indicated that NEDD8 modification of Cul 5 was increased under hypoxia, which could be reversed by pevonedistat.

Here, we investigated whether inactivating Cul 5 by pevonedistat could reverse HPH *in vivo*. To investigate whether pevonedistat could alleviate pulmonary vascular remodeling, we administered pevonedistat (30 mg/kg per dose, once a day, 5 days a week for 4 weeks) to C57BL/6 mice via intraperitoneal injection at the indicated time-points during hypoxia exposure. The mice were randomly divided into four groups: N4W, N4W+ pevonedistat, H4W, and H4W+ pevonedistat.

Pevonedistat alleviated HPH, indicated by an increase in RVSP relative to saline treatment (Figure 4B). Vascular remodeling of PH is mainly seen in distal pulmonary arterioles, so the %MT of <100 μm intrapulmonary arterioles was calculated. Pulmonary morphometrics displayed extenuated pulmonary vascular remodeling in H4W+ pevonedistat group relative to the H4W group (Figure 4C). Hypoxia obviously induced <100 μm intra pulmonary arteriole remodeling, and pevonedistat significantly reversed hypoxic pulmonary vascular remodeling, especially for the <50 μm intrapulmonary arteriole, indicated by an obvious decrease in %MT and MA in pevonedistat-treated arterioles <100 μm.

Pulmonary vascular remodeling can lead to not only increased pulmonary arterial pressure, but also right ventricular hypertrophy,[17] so we evaluated the right ventricle of the mice. The results of wheat germ agglutinin (WGA) and H&E staining (Figure 5A) showed that the cardiomyocyte hypertrophy of the right ventricle was obvious in hypoxia-exposed mice, which could be reversed by pevonedistat. However, the same phenomenon was not observed in cardiomyocytes of the left ventricle. As shown in Figure 5B, hypoxia induced obvious right ventricular hypertrophy, implied by an increase in RVHI and RV/BW ratio, which could also be mitigated by pevonedistat.

Cul 5 participates in endothelial dysfunction *in vitro*

PAEC dysfunction is an important initiating factor for pulmonary vascular remodeling, and Cul 5 is mainly distributed along the endothelium of pulmonary arterioles. Therefore, we investigated the role of Cul 5 on the functions of PAECs. First, we found that silencing of Cul5 could reverse hypoxia-induced increase of EC angiogenesis (Figure 6A, a) and adhesion (Figure 6A, b). Second, we proved that Cul 5 (10 ng/mL) enhances the angiogenesis and adhesion capacity of PAECs, which could be reversed by silencing of NEDD8 and pevonedistat treatment (Figures 6B and 6C). In summary, Cul 5 promotes EC angiogenesis and adhesion capacity, and inhibiting Cul 5 NEDDylation alleviates Cul 5-mediated endothelial dysfunction *in vitro*.

TRAF6/NF-κB/HIF-1α/VEGF pathway is involved in the Cul 5-induced HPH aggravation process

The aforementioned results showed that Cul 5 played a role in pulmonary vascular remodeling during HPH both *in vitro* and *in vivo*, and we investigated the potential mechanism. Our results indicated that Cul 5 participated in HPH via the TRAF6/NF-κB/HIF-1α/VEGF pathway.

As shown in Figure 7A, the expression of the TRAF6/NF-κB/HIF-1α/VEGF pathway was upregulated in H4W mice compared with N4W mice (Figure 7A, a). Pevonedistat treatment reversed the upregulated expression of the TRAF6/NF-κB/HIF-1α/VEGF pathway in H4W mice (Figure 7A, b). *In vitro*, the TRAF6/NF-κB/HIF-1α/VEGF pathway was upregulated by Cul 5 treatment under both normoxia and hypoxia (Figure 7B).

Next, we proved that there is an interaction between Cul-5 and TRAF6 (Figure 8A). TRAF6 is a RING domain ubiquitin ligase that uses the E2 enzyme Ubc13/Uev1A for its autoubiquitination. We then performed ubiquitination assays to determine whether Cul-5 could promote TRAF6 ubiquitination. The results from *in vitro* ubiquitination assays showed that the Cul-5–TRAF6 interaction promotes TRAF6 ubiquitination to mediate NF-kB activation (Figure 8B).

We demonstrated the regulatory effect of Cul 5 on the TRAF6/NF-κB/HIF-1α/VEGF pathway further. TRAF6 inhibitor suppressed the protein expression of TRAF6, NF-κB, HIF-1α and VEGF induced by Cul 5 treatment (Figure 8C). The NF-κB inhibitor suppressed the protein expression of NF-κB, HIF-1α and VEGF induced by Cul 5 treatment (Figure 8D).

Finally, the role of the TRAF6/NF-κB/HIF-1α/VEGF pathway in Cul 5-mediated endothelial dysfunction was investigated. TRAF6/NF-κB/HIF-1α/VEGF pathway blockade could mitigate Cul 5-mediated EC adhesion and angiogenesis (Figure 9). All these results indicate that the TRAF6/NF-κb/HIF-1α/VEGF pathway is involved in the Cul 5-induced HPH aggravation process.

DISCUSSION

The role of Cul 5 in vascular diseases, especially PH, is under clarification. This study found that (1) Cul 5 was upregulated in endothelial cells exposed to hypoxia and in the pulmonary endothelium during HPH pathogenesis; (2) Cul 5 played an important role in the endothelial

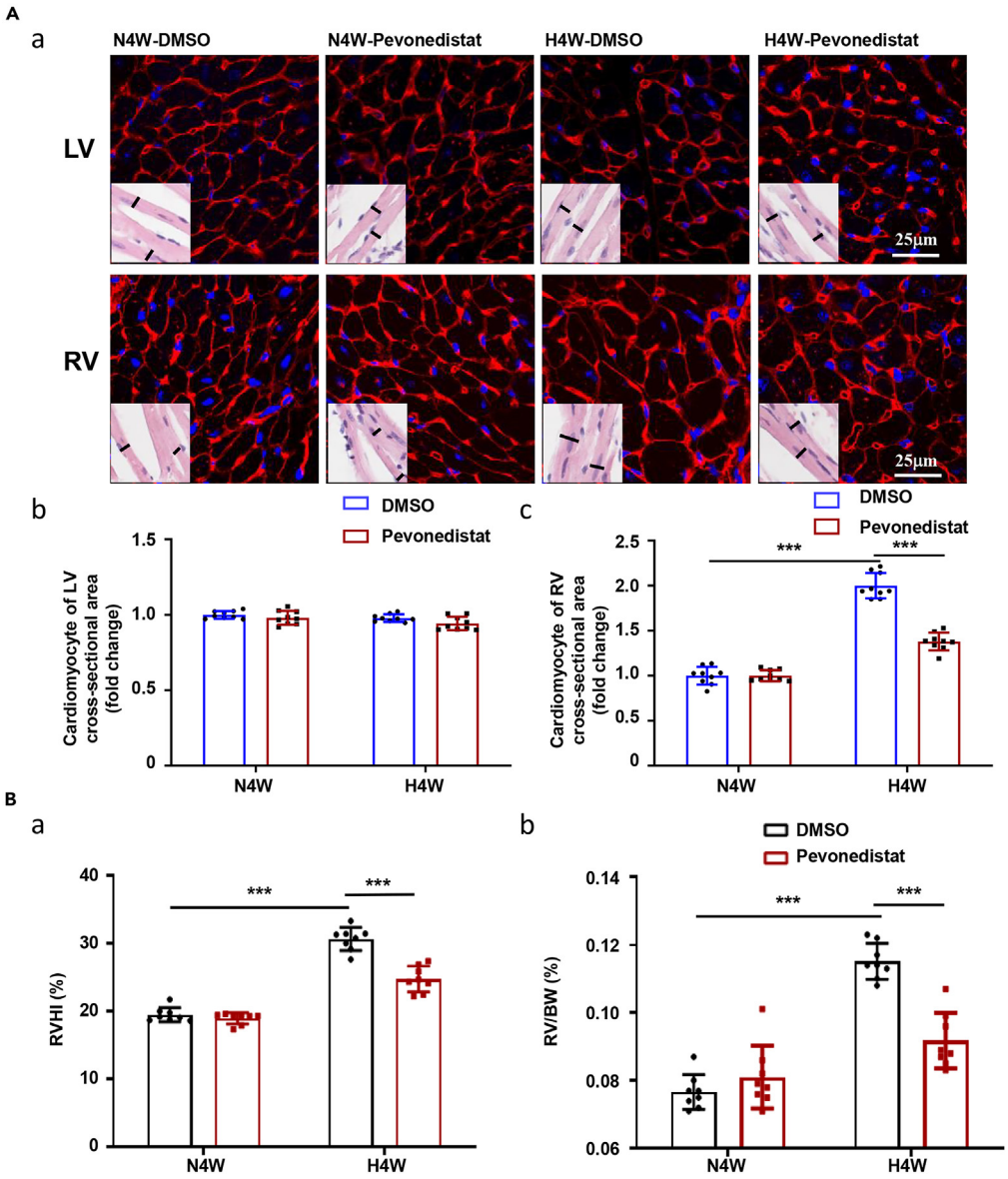

Figure 5. Alleviation effect of Cul 5 inactivator pevonedistat on right ventricular hypertrophy of HPH mice

(A, a) Representative WGA and H&E staining of the left ventricle right (upper panel) and the ventricle (lower panel) derived from N4W + DMSO, N4W + pevonedistat, H4W + DMSO, and H4W + pevonedistat groups. Scale bars: 25 μm. (A, b and c) Cadiomyocyte diameter in the left ventricle and right ventricle in each group.

(B) Right ventricular hypertrophy of the above groups. (a) RVHI of mice; (b) RV/BW ratio of mice. ***$p < 0.001$. Data are represented as the means ± SD, one-way ANOVA was used for statistical analysis in Figure 5.

dysfunction-mediated pulmonary vascular remodeling of HPH; (3) inactivating Cul 5 could alleviate hypoxic pulmonary vascular remodeling; and (4) the Culin5/TRAF6/NF-κB/HIF-1α/VEGF pathway was involved in HPH pathogenesis. To our knowledge, this is the first report to demonstrate that Cul 5 is involved in endothelial dysfunction-mediated pulmonary vascular remodeling of HPH via the TRAF6/NF-κB/HIF-1α/VEGF pathway, suggesting the therapeutic potential of targeting Cul 5 for HPH.

Endothelial dysfunction is thought to be a major contributor to the overall pathogenesis of PH; it is an initiating event of PH under various genetic and exogenous stresses, yet endothelial dysfunction in PH remains incompletely defined.[18,19] Rescuing dysfunctional EC signaling could prevent and reverse PH,[20] and it has been reported that low-dose FK506 prevented exaggerated HPH via induction of EC targets of BMP signaling.[4] PFKFB3-mediated endothelial glycolysis plays a critical role in the development of PH, and targeting PFKFB3 prevents PH development.[21] Arginase inhibition improves NO bioavailability and thereby attenuates endothelial dysfunction, which reverses PH in

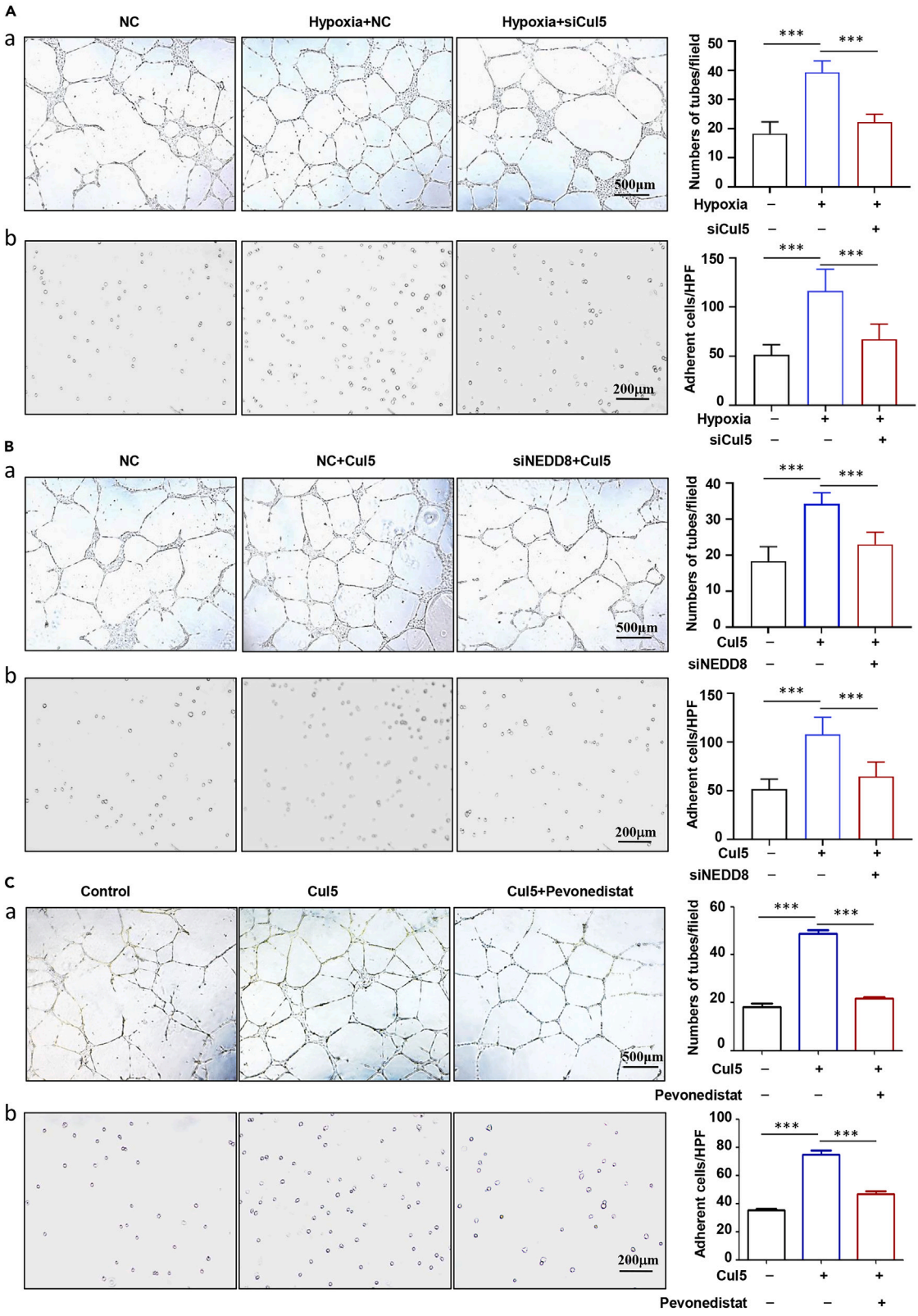
A
a
NC
Hypoxia+NC
Hypoxia+siCul5
500μm
Numbers of tubes/flield
***
***
Hypoxia
siCul5
b
200μm
Adherent cells/HPF
B
NC
NC+Cul5
siNEDD8+Cul5
Cul5
siNEDD8
C
Control
Cul5
Cul5+Pevonedistat
Pevonedistat

Figure 6. Endothelial dysfunction induced by Cul 5 that could be reversed by siNEDD8 silence of pevonedistat treatment

(A) The effect of Cul 5 silence on hypoxia-induced endothelial cell dysfunction. (a) Spontaneous formation of capillaries by HPAECs cultured under hypoxia or normoxia with or without Cul 5 silence for 24 h. The result is expressed as the numbers of tubes per field. ***p < 0.001. Scale bars: 500 μm. (b) Adhesion of HPAECs to culture plate wells when treated under hypoxia or normoxia with or without Cul 5 silence for 24 h. Adherent cells were counted and expressed as the mean numbers of cells per high power field. ***p < 0.001. Scale bars: 200 μm.

(B) The effect of siNEDD8 silence on Cul 5-induced endothelial cell dysfunction. (a) Spontaneous formation of capillaries by HPAECs treated with or without Cul 5 or siNEDD8 silence for 24 h. The result is expressed as the numbers of tubes per field. ***p < 0.001. Scale bars: 500 μm. (b) Adhesion of HPAECs to culture plate wells when treated with or without Cul 5 or siNEDD8 silence for 24 h. Adherent cells were counted and expressed as the mean numbers of cells per high power field. ***p < 0.001. Scale bars: 200 μm.

(C) The effect of pevonedistat on Cul 5-induced endothelial cell dysfunction. (a) Spontaneous formation of capillaries by HPAECs treated with or without Cul 5 or pevonedistat for 24 h. The result is expressed as the numbers of tubes per field. ***p < 0.001. Scale bars: 500 μm. (b) Adhesion of HPAECs to culture plate wells when treated with or without Cul 5 or pevonedistat for 24 h. Adherent cells were counted and expressed as the mean numbers of cells per high power field. ***p < 0.001. Scale bars: 200 μm. Data are represented as the means ± SD, one-way ANOVA was used for statistical analysis in Figure 6.

transgenic sickle cell mice.[22] Improving EndoMT-mediated endothelial dysfunction can also attenuate PH.[23] In this study, we showed that Cul 5 upregulation induced endothelial dysfunction and that Cul 5 inactivation improved endothelial dysfunction, thereby reversing hypoxic pulmonary vascular remodeling. Our results provide a potential treatment target for HPH.

Seven different types of Cul proteins have been identified in human cells (Cul 1, Cul 2, Cul 3, Cul 4A, Cul 4B, Cul 5, Cul 7, and Cul 9), each of which engages a family of substrate receptors to assemble active CRLs, which are crucial in the cardiovascular system.[24] In addition, Cul 5 has been identified to play positive roles in regulating cell growth, proliferation and physiological and other processes in the human body[25] and is expressed in many cells and organs, including endothelial cells, brain, kidney collecting tubule cells, and vascular endothelial cells.[11,26] While the importance of CRL5-dependent protein ubiquitination in cancers has been well-documented,[27] what role each CRL5 plays in the cardiovascular system has just started to come to light, our study demonstrated for the first time that Cul 5 participates in the pathogenesis of HPH. Cul 5 has been confirmed to regulate EC growth and may modulate angiogenesis.[28] We also showed that Cul 5 could induce PAEC angiogenesis and adhesion ability. It has been reported that Cul5 plays a role in EC growth and angiogenesis by regulating MAPK phosphorylation the nuclear localization of EGR-1, maspin expression, and actin polymerization,[28–30] while the underlying mechanisms remain to unclear.

TRAF6 is a substrate of Cul 5,[25] and it has also been reported that the Cul 5—TRAF6 interaction activates NF-κB signaling.[12] The TRAF6/NF-κB pathway is involved in many diseases, such as cancer,[31] lung injury,[32] and myocardial injury.[33] A previous study showed that TRAF was upregulated in idiopathic pulmonary arterial hypertension patients,[34] while its regulatory mechanisms and its role in HPH are unclear. Our study confirmed for the first time that the Cul 5—TRAF6 interaction activates NF-κB/HIF-1α/VEGF to mediate endothelial dysfunction and then leads to pulmonary vascular remodeling, revealing the pathogenesis of HPH and providing a potential treatment target.

Cul 5 is currently regarded as a promising drug target molecule because of its various biological roles.[25] In this study we showed that Cul 5 promotes angiogenesis and cell adhesion. Cul 5 is the key component of Cullin-RING ligase-5 (CRL-5), and activation of CRL-5 requires Cul 5 neddylation, which is catalyzed by a neddylation enzyme cascade, consisting of the E1 NEDD8-activating enzyme, the E2 neddylation conjugating enzyme, and E3 neddylation ligase,[35,36] thus, neddylation inhibitor could inactive Cul 5. Inactivating Cul 5 treatment by pevonedistat (first-in-class neddylation inhibitor) is an attractive pharmacological intervention in many diseases. Pevonedistat decreases neddylation of the Cul 5 protein and subsequently suppresses p53 degradation, which impedes efficient adenoviruses replication.[37] It has also been reported that pevonedistat targets Cul 5 to change the functions of TRAF6 to mitigate lipopolysaccharide-induced acute lung injury (ALI), providing a therapeutic intervention for ALI.[12] In glioma patients, Cul 5 expression was inversely correlated with anti-angiogenic vHL protein and important oncogenic transcriptional factor p65/RelA. Pevonedistat can downregulate CRL5 activity, which may be a promising therapeutic approach in glioblastoma.[38] In the present study, we demonstrated that pevonedistat could alleviate Cul 5-mediated endothelial dysfunction *in vitro and* alleviate HPH *in vivo*, shedding light on potential, future HPH treatment.

In conclusion, this work implicates Cul 5 as a mediator of HPH via the TRAF6/NF-κB/HIF-1α/VEGF pathway, which could be considered a potential therapeutic target in the clinical treatment of HPH. Thus, it is necessary to develop CRL5-specific inhibitors for potential therapeutic management of HPH.

Limitations of the study

We recognized the important role of Cul 5 in HPH by in silico predictions, and validation was performed. Our study also has certain limitations. First, the upregulation of Cul 5 needs to be validated in larger clinical samples. Second, we only investigated the downstream molecular mechanisms of Cul 5, the upstream regulatory mechanisms of Cul 5 upregulation need future research. Third, the effect of more Cul 5 blockade methodson HPH development needs to be validated. Finally, the interaction mechanism of Cul 5 and TRAF6 requires further study.

STAR★METHODS

Detailed methods are provided in the online version of this paper and include the following:

- KEY RESOURCES TABLE
- RESOURCE AVAILABILITY

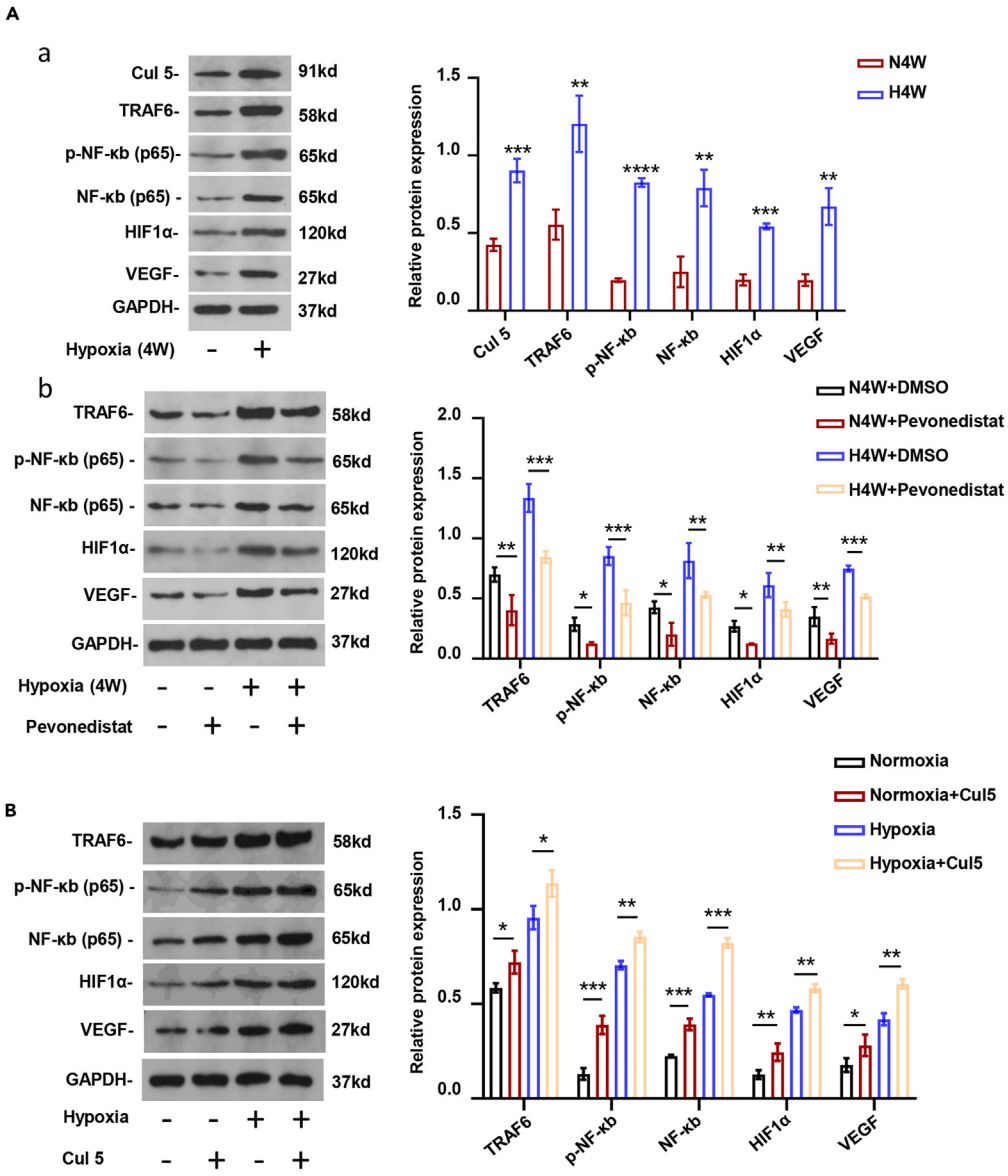

Figure 7. Upregulated expression of TRAF6/NF-κB/HIF-1α/VEGF pathway in HPH that aggravated by Cul 5 further

(A) The effect of hypoxia treatment for 4 weeks on Cul5/TRAF6/NF-κB/HIF-1α/VEGF pathway expression in lung tissues of mice, and reverse effect of pevonedistat. (a) Western blot analysis of TRAF6/NF-κB/HIF-1α/VEGF pathway expression in N4W and H4W group and statistical analysis of the proteins relative expression normalized to GAPDH. (b) Western blot analysis of TRAF6/NF-κB/HIF-1α/VEGF pathway expression in N4W + DMSO, N4W + pevonedistat, H4W+ DMSO, and H4W + pevonedistat group, and statistical analysis of the proteins relative expression normalized to GAPDH.

(B) The effect of hypoxia and/or Cul 5 treatment on TRAF6/NF-κB/HIF-1α/VEGF pathway expression in PAECs. Western blot analysis of TRAF6/NF-κB/HIF-1α/VEGF pathway expression in endothelial cells exposed to normoxia and hypoxia with or without Cul 5, and statistical analysis of the proteins relative expression normalized to GAPDH. *$p < 0.05$, **$p < 0.01$, ***$p < 0.001$. Student's *t* test was used for statistical analysis in Figure 7A(a). Data are represented as the means ± SD, one-way ANOVA was used for statistical analysis in Figure 7A(b) and 7B.

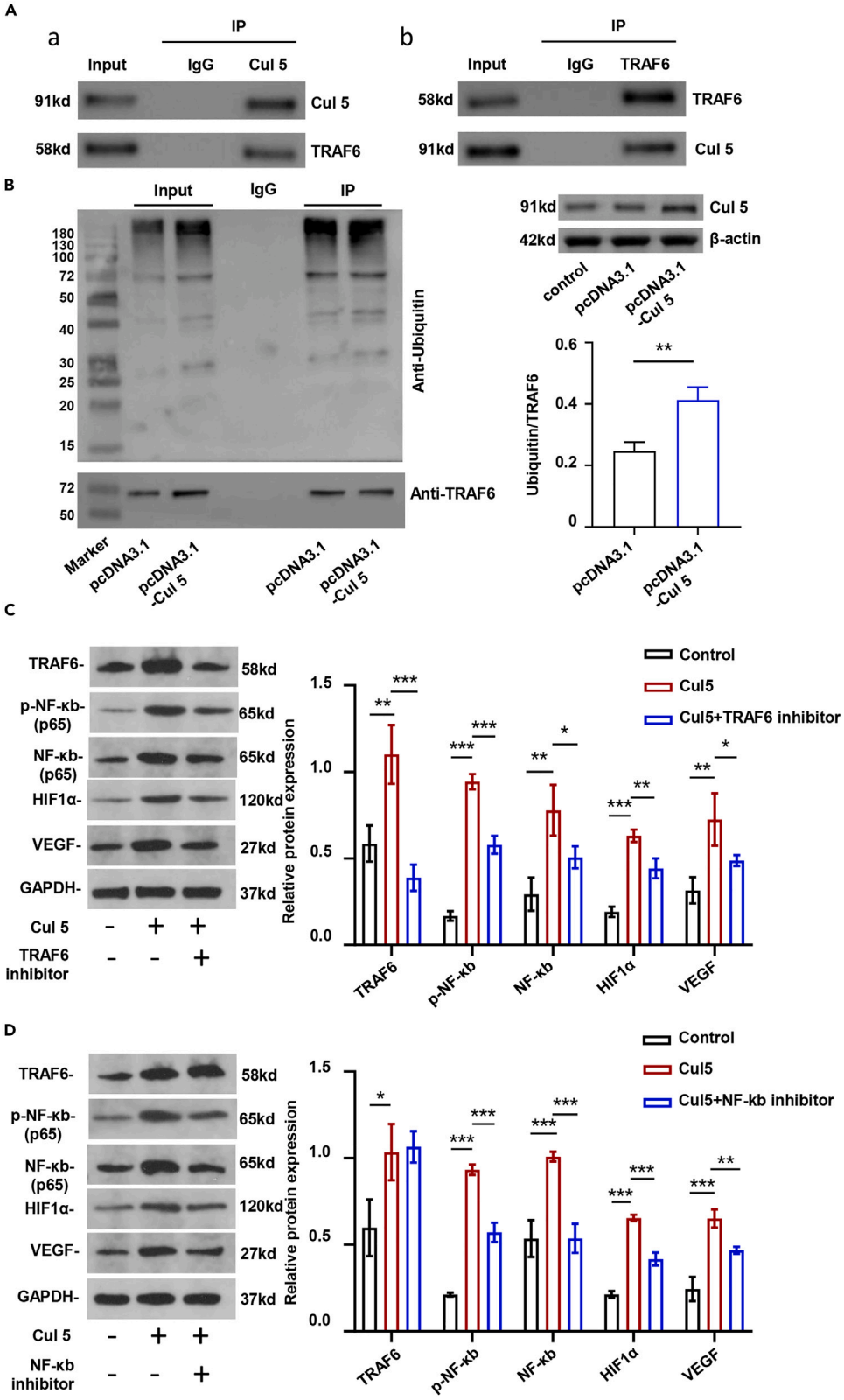
A
a
IP
Input
IgG
Cul 5
91kd
Cul 5
58kd
TRAF6
b
IP
Input
IgG
TRAF6
58kd
TRAF6
91kd
Cul 5
B
Input
IgG
IP
180
130
100
72
50
40
30
25
20
15
Anti-Ubiquitin
72
50
Anti-TRAF6
Marker
pcDNA3.1
pcDNA3.1 -Cul 5
pcDNA3.1
pcDNA3.1 -Cul 5
91kd
Cul 5
42kd
β-actin
control
pcDNA3.1
pcDNA3.1 -Cul 5
Ubiquitin/TRAF6
0.6
0.4
0.2
0
**
pcDNA3.1
pcDNA3.1 -Cul 5
C
TRAF6-
58kd
p-NF-κb-(p65)
65kd
NF-κb-(p65)
65kd
HIF1α-
120kd
VEGF-
27kd
GAPDH-
37kd
Cul 5 - + +
TRAF6 inhibitor - - +
Relative protein expression
1.5
1.0
0.5
0.0
Control
Cul5
Cul5+TRAF6 inhibitor
TRAF6
p-NF-κb
NF-κb
HIF1α
VEGF
D
TRAF6-
58kd
p-NF-κb-(p65)
65kd
NF-κb-(p65)
65kd
HIF1α-
120kd
VEGF-
27kd
GAPDH-
37kd
Cul 5 - + +
NF-κb inhibitor - - +
Relative protein expression
1.5
1.0
0.5
0.0
Control
Cul5
Cul5+NF-kb inhibitor
TRAF6
p-NF-κb
NF-κb
HIF1α
VEGF

Figure 8. Activation of TRAF6/NF-κB/HIF-1α/VEGF pathway by Cul 5

(A) Interaction between Cul 5 and TRAF6. (a and b) Co-IP of Cul-5 with TRAF6 in the lysate from PAECs cells. Cell lysates were prepared (input, left panel) and immunoprecipitations (IP, right panel) were performed with anti-Cul 5 or anti-TRAF6 antibody. Normal IgG (IgG, middle panel) was used as a negative control for IP. Cell lysates and immunoprecipitates were analyzed with anti-Cul 5 and anti-TRAF6.

(B) Promotion of TRAF6 ubiquitination induced by Cul 5 overexpression. Cell lysates were prepared (input, left panel) and immunoprecipitations (IP, right panel) were performed with anti-TRAF6 antibody. Normal IgG (IgG, middle panel) was used as a negative control for IP. Cell lysates and immunoprecipitates were analyzed with anti-TRAF6 and anti-ubiquitin. Quantification of immunoprecipitated TRAF6 and ubiquitin. Data are represented as the means ± SD of three separate experiments. $^{**}p < 0.01$. Student's *t* test was used for statistical analysis.

(C) Western blot analysis of TRAF6/NF-κB/HIF-1α/VEGF pathway expression in endothelial cells treated by Cul 5 and TRAF6 inhibitor, and statistical analysis of the proteins relative expression normalized to GAPDH. The three groups are Control, Cul 5, and Cul 5+ TRAF6 inhibitor. $^{*}p < 0.05$, $^{**}p < 0.01$, $^{***}p < 0.001$. Data are represented as the means ± SD, one-way ANOVA was used for statistical analysis.

(D) Western blot analysis of TRAF6/NF-κB/HIF-1α/VEGF pathway expression in endothelial cells treated by Cul 5 and NF-κB inhibitor, and statistical analysis of the proteins relative expression normalized to GAPDH. The three groups are Control, Cul 5, and Cul 5+ NF-κB inhibitor. $^{*}p < 0.05$, $^{**}p < 0.01$, $^{***}p < 0.001$. Data are represented as the means ± SD, one-way ANOVA was used for statistical analysis.

SUPPLEMENTAL INFORMATION

Supplemental information can be found online at https://doi.org/10.1016/j.isci.2023.108199.

ACKNOWLEDGMENTS

National Natural Science Foundation of China (82270055 and 82241011), Natural Science Foundation of Shaanxi Province (2022JQ-761 and 2022JQ-940), and Chinese Postdoctoral Science Foundation (2021M702610).

AUTHOR CONTRIBUTIONS

L.W., J.L., W.W., S.Y., and C.W. designed the experiments; L.W., J.H., R.Z., M.Z., and C.L. conducted the experiments, collected, analyzed data and Y.L. participated in supplementary experiments advised by editors; L.W. wrote the paper. All authors reviewed the manuscript.

DECLARATION OF INTERESTS

The authors declare no competing interests.

INCLUSION AND DIVERSITY

We support inclusive, diverse, and equitable conduct of research.

Received: April 25, 2023
Revised: May 5, 2023
Accepted: October 10, 2023
Published: October 12, 2023

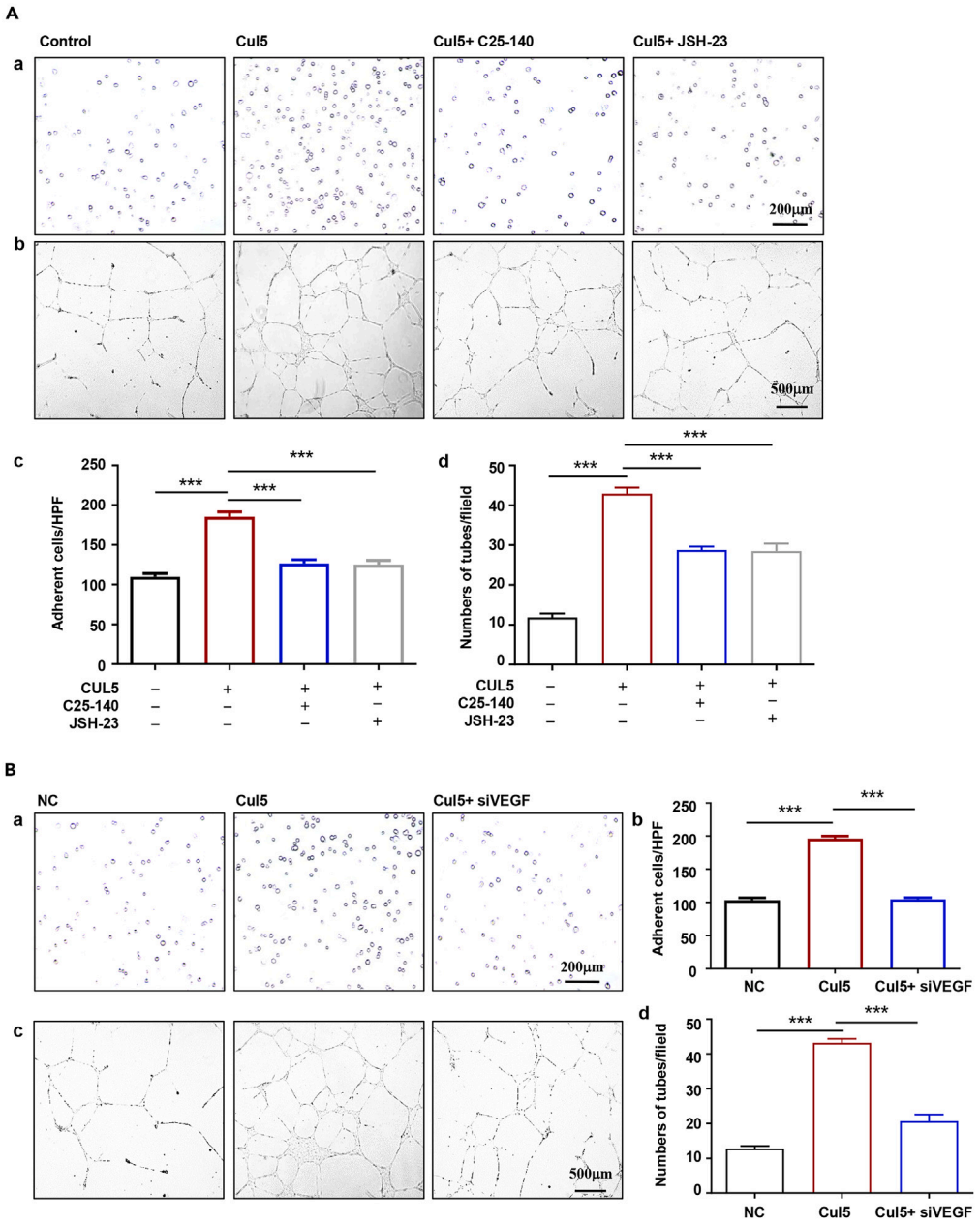

Figure 9. Alleviation effect of TRAF6/NF-κB/HIF-1α/VEGF pathway blockade on Cul 5-induced endothelial cell dysfunctions

(A) Effect of TRAF6 or NF-κB blocker on Cul 5-induced endothelial cell dysfunctions. (a and c) Adhesion of HPAECs to culture plate wells of Control, Cul 5, Cul 5 + C25-140, and Cul 5+JSH-23. Adherent cells were counted and expressed as the mean numbers of cells per high power field. ***$p < 0.001$. Scale bars: 200 μm. Data are represented as the means ± SD, one-way ANOVA was used for statistical analysis. (b and d) Spontaneous formation of capillaries by HPAECs of the above groups. The result is expressed as the numbers of tubes per field. ***$p < 0.001$. Scale bars: 500 μm. Data are represented as the means ± SD, one-way ANOVA was used for statistical analysis.

(B) Effect of VEGF knockdown by siRNA on Cul 5-induced endothelial cell dysfunctions. (a and b) Adhesion of HPAECs to culture plate wells of Control, Cul 5, and Cul 5+siVEGF. Adherent cells were counted and expressed as the mean numbers of cells per high power field. ***$p < 0.001$. Scale bars: 200 μm. Data are represented as the means ± SD, one-way ANOVA was used for statistical analysis. (c and d) Spontaneous formation of capillaries by HPAECs of the three groups. The result is expressed as the numbers of tubes per field. ***$p < 0.001$. Scale bars: 500 μm. Data are represented as the means ± SD, one-way ANOVA was used for statistical analysis.

REFERENCES

1. Simonneau, G., Montani, D., Celermajer, D.S., Denton, C.P., Gatzoulis, M.A., Krowka, M., Williams, P.G., and Souza, R. (2019). Haemodynamic definitions and updated clinical classification of pulmonary hypertension. Eur. Respir. J. *53*, 1801913. https://doi.org/10.1183/13993003.01913-2018.
2. Tuder, R.M. (2017). Pulmonary vascular remodeling in pulmonary hypertension. Cell Tissue Res. *367*, 643–649. https://doi.org/10.1007/s00441-016-2539-y.
3. Ranchoux, B., Harvey, L.D., Ayon, R.J., Babicheva, A., Bonnet, S., Chan, S.Y., Yuan, J.X.J., and Perez, V.d.J. (2018). Endothelial dysfunction in pulmonary arterial hypertension: an evolving landscape (2017 Grover Conference Series). Pulm. Circ. *8*, 2045893217752912. https://doi.org/10.1177/2045893217752912.
4. Spiekerkoetter, E., Tian, X., Cai, J., Hopper, R.K., Sudheendra, D., Li, C.G., El-Bizri, N., Sawada, H., Haghighat, R., Chan, R., et al. (2013). FK506 activates BMPR2, rescues endothelial dysfunction, and reverses pulmonary hypertension. J. Clin. Invest. *123*, 3600–3613. https://doi.org/10.1172/JCI65592.
5. Long, L., Ormiston, M.L., Yang, X., Southwood, M., Gräf, S., Machado, R.D., Mueller, M., Kinzel, B., Yung, L.M., Wilkinson, J.M., et al. (2015). Selective enhancement of endothelial BMPR-II with BMP9 reverses pulmonary arterial hypertension. Nat. Med. *21*, 777–785. https://doi.org/10.1038/nm.3877.
6. Olsson, A.K., Dimberg, A., Kreuger, J., and Claesson-Welsh, L. (2006). VEGF receptor signalling - in control of vascular function. Nat. Rev. Mol. Cell Biol. *7*, 359–371. https://doi.org/10.1038/nrm1911.
7. Masri, F.A., Anand-Apte, B., Vasanji, A., Xu, W., Goggans, T., Drazba, J., and Erzurum, S.C. (2005). Definitive evidence of fundamental and inherent alteration in the phenotype of primary pulmonary hypertension endothelial cells in angiogenesis. Chest *128*, 571S. https://doi.org/10.1378/chest.128.6_suppl.571S.
8. Gallardo-Vara, E., Ntokou, A., Dave, J.M., Jovin, D.G., Saddouk, F.Z., and Greif, D.M. (2023). Vascular pathobiology of pulmonary hypertension. J. Heart Lung Transplant. *42*, 544–552. https://doi.org/10.1016/j.healun.2022.12.012.
9. Liu, J., Wang, W., Wang, L., Chen, S., Tian, B., Huang, K., Corrigan, C.J., Ying, S., Wang, W., and Wang, C. (2018). IL-33 Initiates Vascular Remodelling in Hypoxic Pulmonary Hypertension by up-Regulating HIF-1alpha and VEGF Expression in Vascular Endothelial Cells. EBioMedicine *33*, 196–210. https://doi.org/10.1016/j.ebiom.2018.06.003.
10. Burnatowska, H., Zeneberg, A., Roulo, A., Grobe, J., Zhao, P., Lelkes, P.I., Clare, P., and Barney, C. (2001). Expression of VACM-1 protein in cultured rat adrenal endothelial cells is linked to the cell cycle. Endothelium *8*, 49–63.
11. Burnatowska-Hledin, M.A., and Barney, C.C. (2014). New insights into the mechanism for VACM-1/cul5 expression in vascular tissue in vivo. Int. Rev. Cell Mol. Biol. *313*, 79–101. https://doi.org/10.1016/B978-0-12-800177-6.00003-7.
12. Zhu, Z., Sun, L., Hao, R., Jiang, H., Qian, F., and Ye, R.D. (2017). Nedd8 modification of Cullin-5 regulates lipopolysaccharide-induced acute lung injury. Am. J. Physiol. Lung Cell Mol. Physiol. *313*, L104–L114. https://doi.org/10.1152/ajplung.00410.2016.
13. van Uden, P., Kenneth, N.S., and Rocha, S. (2008). Regulation of hypoxia-inducible factor-1alpha by NF-kappaB. Biochem. J. *412*, 477–484. https://doi.org/10.1042/BJ20080476.
14. Santosh, S., Chu, C., Mwangi, J., Narayan, M., Mosman, A., Nayak, R., and Philipneri, M. (2019). Changes in pulmonary artery systolic pressure and right ventricular function in patients with end-stage renal disease on maintenance dialysis. Nephrology *24*, 74–80. https://doi.org/10.1111/nep.13183.
15. Enchev, R.I., Schulman, B.A., and Peter, M. (2015). Protein neddylation: beyond cullin-RING ligases. Nat. Rev. Mol. Cell Biol. *16*, 30–44. https://doi.org/10.1038/nrm3919.
16. Foster, J.H., Barbieri, E., Zhang, L., Scorsone, K.A., Moreno-Smith, M., Zage, P., and Horton, T.M. (2021). The Anti-Tumor Activity of the NEDD8 Inhibitor Pevonedistat in Neuroblastoma. Int. J. Mol. Sci. *22*, 6565. https://doi.org/10.3390/ijms22126565.
17. Chouvarine, P., Photiadis, J., Cesnjevar, R., Scheewe, J., Bauer, U.M.M., Pickardt, T., Kramer, H.H., Dittrich, S., Berger, F., and Hansmann, G. (2021). RNA expression profiles and regulatory networks in human right ventricular hypertrophy due to high pressure load. iScience *24*, 102232. https://doi.org/10.1016/j.isci.2021.102232.
18. Yu, Q., and Chan, S.Y. (2017). Mitochondrial and Metabolic Drivers of Pulmonary Vascular Endothelial Dysfunction in Pulmonary Hypertension. Adv. Exp. Med. Biol. *967*, 373–383. https://doi.org/10.1007/978-3-319-63245-2_24.
19. Loscalzo, J. (1992). Endothelial dysfunction in pulmonary hypertension. N. Engl. J. Med. *327*, 117–119. https://doi.org/10.1056/NEJM199207093270209.
20. Risbano, M.G., and Gladwin, M.T. (2013). Therapeutics targeting of dysregulated redox equilibrium and endothelial dysfunction. Handb. Exp. Pharmacol. *218*, 315–349. https://doi.org/10.1007/978-3-642-38664-0_13.
21. Cao, Y., Zhang, X., Wang, L., Yang, Q., Ma, Q., Xu, J., Wang, J., Kovacs, L., Ayon, R.J., Liu, Z., et al. (2019). PFKFB3-mediated endothelial glycolysis promotes pulmonary hypertension. Proc. Natl. Acad. Sci. USA *116*, 13394–13403. https://doi.org/10.1073/pnas.1821401116.
22. Steppan, J., Tran, H.T., Bead, V.R., Oh, Y.J., Sikka, G., Bivalacqua, T.J., Burnett, A.L., Berkowitz, D.E., and Santhanam, L. (2016). Arginase Inhibition Reverses Endothelial Dysfunction, Pulmonary Hypertension, and Vascular Stiffness in Transgenic Sickle Cell Mice. Anesth. Analg. *123*, 652–658. https://doi.org/10.1213/ANE.0000000000001378.
23. Shi, R., Zhu, D., Wei, Z., Fu, N., Wang, C., Liu, L., Zhang, H., Liang, Y., Xing, J., Wang, X., and Wang, Y. (2018). Baicalein attenuates monocrotaline-induced pulmonary arterial hypertension by inhibiting endothelial-to-mesenchymal transition. Life Sci. *207*, 442–450. https://doi.org/10.1016/j.lfs.2018.06.033.
24. Diaz, S., Wang, K., Sjögren, B., and Liu, X. (2022). Roles of Cullin-RING Ubiquitin Ligases in Cardiovascular Diseases. Biomolecules *12*, 416. https://doi.org/10.3390/biom12030416.
25. Bano, I., Soomro, A.S., Abbas, S.Q., Ahmadi, A., Hassan, S.S.U., Behl, T., and Bungau, S. (2022). A Comprehensive Review of Biological Roles and Interactions of Cullin-5 Protein. ACS Omega *7*, 5615–5624. https://doi.org/10.1021/acsomega.1c06890.
26. Okumura, F., Joo-Okumura, A., Nakatsukasa, K., and Kamura, T. (2016). The role of cullin 5-containing ubiquitin ligases. Cell Div. *11*, 1. https://doi.org/10.1186/s13008-016-0016-3.
27. Zhao, Y., Xiong, X., and Sun, Y. (2020). Cullin-RING Ligase 5: Functional characterization and its role in human cancers. Semin. Cancer Biol. *67*, 61–79. https://doi.org/10.1016/j.semcancer.2020.04.003.
28. Buchwalter, A., Van Dort, C., Schultz, S., Smith, R., Le, I.P., Abbott, J.L., Oosterhouse, E., Johnson, A.E., Hansen-Smith, F., and Burnatowska-Hledin, M. (2008). Expression of VACM-1/cul5 mutant in endothelial cells induces MAPK phosphorylation and maspin degradation and converts cells to the angiogenic phenotype. Microvasc. Res. *75*, 155–168. https://doi.org/10.1016/j.mvr.2007.08.004.
29. Bradley, S.E., Johnson, A.E., Le, I.P., Oosterhouse, E., Hledin, M.P., Marquez, G.A., and Burnatowska-Hledin, M. (2010). Phosphorylation of VACM-1/Cul5 by protein kinase A regulates its neddylation and antiproliferative effect. J. Biol. Chem. *285*, 4883–4895. https://doi.org/10.1074/jbc.M109.085225.
30. Zou, Z., Anisowicz, A., Hendrix, M.J., Thor, A., Neveu, M., Sheng, S., Rafidi, K., Seftor, E., and Sager, R. (1994). Maspin, a serpin with tumor-suppressing activity in human mammary epithelial cells. Science *263*, 526–529. https://doi.org/10.1126/science.8290962.
31. Guangwei, Z., Zhibin, C., Qin, W., Chunlin, L., Penghang, L., Ruofan, H., Hui, C., Hoffman, R.M., and Jianxin, Y. (2022). TRAF6 regulates the signaling pathway influencing colorectal cancer function through ubiquitination mechanisms. Cancer Sci. *113*, 1393–1405. https://doi.org/10.1111/cas.15302.
32. Liu, X., Lin, Z., and Xu, Y. (2021). Pellino1 promoted inflammation in lung injury model of sepsis by TRAF6/NF-kappaB signal pathway. J. Inflamm. *18*, 11. https://doi.org/10.1186/s12950-021-00276-6.
33. Li, Y., Zhang, L., Zhang, P., and Hao, Z. (2021). Dehydrocorydaline Protects Against Sepsis-Induced Myocardial Injury Through Modulating the TRAF6/NF-kappaB Pathway. Front. Pharmacol. *12*, 709604. https://doi.org/10.3389/fphar.2021.709604.
34. Chouvarine, P., Legchenko, E., Geldner, J., Riehle, C., and Hansmann, G. (2019). Hypoxia drives cardiac miRNAs and inflammation in the right and left ventricle. J. Mol. Med. *97*, 1427–1438. https://doi.org/10.1007/s00109-019-01817-6.
35. Zhang, S., and Sun, Y. (2020). Cullin RING Ligase 5 (CRL-5): Neddylation Activation and Biological Functions. Adv. Exp. Med. Biol. *1217*, 261–283. https://doi.org/10.1007/978-981-15-1025-0_16.
36. Duda, D.M., Borg, L.A., Scott, D.C., Hunt, H.W., Hammel, M., and Schulman, B.A. (2008). Structural insights into NEDD8 activation of cullin-RING ligases: conformational control of conjugation. Cell *134*, 995–1006. https://doi.org/10.1016/j.cell.2008.07.022.
37. Guo, H., Shen, S., Li, Y., Bi, R., Zhang, N., Zheng, W., Deng, Y., Yang, Y., Yu, X.F., Wang,

C., and Wei, W. (2019). Adenovirus oncoprotein E4orf6 triggers Cullin5 neddylation to activate the CLR5 E3 ligase for p53 degradation. Biochem. Biophys. Res. Commun. *516*, 1242–1247. https://doi.org/10.1016/j.bbrc.2019.07.028.

38. Zheng, S., and Li, Z. (2020). Identification of a cullin5-RING E3 ligase transcriptome signature in glioblastoma multiforme. Aging (Albany NY) *12*, 17380–17392. https://doi.org/10.18632/aging.103737.
39. Zhu, L.J., Li, T.Y., Luo, C.X., Jiang, N., Chang, L., Lin, Y.H., Zhou, H.H., Chen, C., Zhang, Y., Lu, W., et al. (2014). CAPON-nNOS coupling can serve as a target for developing new anxiolytics. Nat. Med. *20*, 1050–1054. https://doi.org/10.1038/nm.3644.
40. Wang, W., Liu, J., Ma, A., Miao, R., Jin, Y., Zhang, H., Xu, K., Wang, C., and Wang, J. (2014). mTORC1 is involved in hypoxia-induced pulmonary hypertension through the activation of Notch3. J. Cell. Physiol. *229*, 2117–2125. https://doi.org/10.1002/jcp.24670.
41. Shi, Y., Liu, J., Zhang, R., Zhang, M., Cui, H., Wang, L., Cui, Y., Wang, W., Sun, Y., and Wang, C. (2023). Targeting Endothelial ENO1 (Alpha-Enolase) -PI3K-Akt-mTOR Axis Alleviates Hypoxic Pulmonary Hypertension. Hypertension *80*, 1035–1047. https://doi.org/10.1161/HYPERTENSIONAHA.122.19857.

STAR★METHODS

KEY RESOURCES TABLE

REAGENT or RESOURCE	SOURCE	IDENTIFIER
Antibodies		
Rabbit monoclonal anti-Cul 5	Abcam	Cat#ab264284; RRID: AB_3073511
Rabbit monoclonal anti-CD31	Abcam	Cat#ab182981; RRID: AB_2920881
Rabbit monoclonal anti-TRAF6	Abcam	Cat#Ab33915; RRID: AB_778572
Rabbit monoclonal anti-NF-κb	Cell Signaling Technology	Cat#8242; RRID: AB_10859369
Rabbit monoclonal anti-VEGF	Affinity Biosciences	Cat#Af5131; RRID: AB_2837617
Rabbit monoclonal anti-p-NF-κb	Affinity Biosciences	Cat#AF2006; RRID: AB_2834435
Mouse monoclonal anti-HIF1 alpha	Affinity Biosciences	Cat#BF8002; RRID: AB_2846221
Rabbit monoclonal anti-GAPDH	Goodhere Biological Technology	Cat#AB-P-R001; RRID: AB_3073512
Mouse monoclonal anti–β-actin	Proteintech	Cat#66009-1-Ig; RRID: AB_2687938
Mouse monoclonal anti-TRAF6	Santa Cruz	Cat#sc-8409; RRID: AB_628391
Rabbit monoclonal anti-Cul 5	Santa Cruz	Cat#sc-373822; RRID: AB_10992228
HRP-conjugated secondary antibody	R&D	Cat#HAF017; RRID: AB_562588
Alex Fluor 488 secondary antibody	ZSGB-BIO	Cat#ZF0511; RRID: AB_2864279
Alex Fluor 594 secondary antibody	ZSGB-BIO	Cat#ZF0516; RRID: AB_2936330
Bacterial and virus strains		
HBAAV2/VEC-TIE-mir30-*m*-CUL5 shRNA-ZsGreenvector	Hanbio Tech	N/A
HBAAV2/VEC-TIE-ZsGreencontrol vector	Hanbio Tech	N/A
Biological samples		
Bronchiectasis/Bronchiectasis-PH patients lung tissues	Beijing Chao-Yang Hospital, Capital Medical University	N/A
Donors lung tissues	Beijing Chao-Yang Hospital, Capital Medical University	N/A
Chemicals, peptides, and recombinant proteins		
Pevonedistat	MCE	Cat#HY-70062
C25-140	MCE	Cat#HY-120934
JSH-23	MCE	Cat#HY-13982
EDTA	Sigma-Aldrich	Cat#EDS-100G
TRIzol reagent	Invitrogen	Cat#15596-026
Critical commercial assays		
RNeasy Mini Kit	Qiagen	Cat#74106
Matrigel	BD	Cat#356234
Fibronectin	MILLIPORE	Cat#FC010
WGA	Invitrogen	Cat#W11262
DAPI	ZSGB-BIO	Cat#ZLI-9557
Electrochemiluminescence (ECL) substrate	Thermo	Cat#34579
IP lysis buffer	abiowell	Cat#AWB0164a
protein G PLUS-Agarose beads	Santa	Cat#sc-2003
16 SDS sample loading buffer	abiowell	Cat#AWB0055
Deposited data		
Raw and analyzed data	This paper	GEO: GSE243567

(*Continued on next page*)

Continued

REAGENT or RESOURCE	SOURCE	IDENTIFIER
Experimental models: Cell lines		
Human PAECs	ScienCell Research Laboratories	Cat#3100
Experimental models: Organisms/strains		
C57BL/6	This paper	www.vitalriver.com
Oligonucleotides		
siRNA targeting sequence: Cul 5 sense:5′ -GGCUAAUAGAGCACAAAUATT-3′ anti-sense:5′ -UAUUUGUGCUCUAUUAGCCCTT-3′	This paper	N/A
siRNA targeting sequence: NEDD8 sense:5′ -GAGAAGACAGCAGCUGAUUTT-3′ anti-sense:5′ -AAUCAGCUGCUGUCUUCUCTT-3′	This paper	N/A
siRNA targeting sequence: VEGFA sense: 5′ -GGCAGCUUGAGUUAAACGATT-3′ anti-sense: 5′ -UCGUUUAACUCAAGCUGCCTT -3′	This paper	N/A
siRNA targeting sequence: Negative control (NC): sense: 5′ -UUCUCCGAACGUGUCACGUTT-3′ anti-sense: 5′ -ACGUGACACGUUCGGAGAATT-3	This paper	N/A
Recombinant DNA		
pcDNA3.1-CUL5-3xFlag-Puro	HonorGene	HG-HO003478
Software and algorithms		
Vevo 2100 high-resolution imaging system	VisualSonics	N/A
LabChart system	ADInstruments	https://www.adinstruments.com/
NIS-Elements Basic Research-Microscope Imaging Software	Nikon	https://www.microscope.healthcare.nikon.com/
ImageJ software	National Institutes of Health	https://ImageJ.nih.gov/ij/
GraphPad Prism version 9.3	GraphPad	https://www.graphpad.com/scientificsoftware/prism/

RESOURCE AVAILABILITY

Lead contact

Further information and requests for resources and reagents should be directed to and will be fulfilled by the lead contact, Jie Liu (liujie@ccmu.edu.cn).

Materials availability

This study did not generate any unique new reagent. All reagents used in this study are commercially available.

Data and code availability

- Microarray data can be accessed in GEO under the accession number: GEO: GSE243567.
- This paper does not report original code.
- Any additional information required to reanalyze the data reported in this paper is available from the lead contact upon request.
- The data used to support the findings of this study are available from the corresponding author upon request.

EXPERIMENTAL MODEL AND STUDY PARTICIPANT DETAILS

Cell culture and preparation

Human PAECs from normal human subjects (ScienCell Research Laboratories, CA, USA, Cat.No.3100) were cultured in culture medium (EC Medium, ECM, ScienCell Research Laboratories, CA, USA, Cat.No.1001), supplemented with Penicillin/Streptomycin (P/S), growth supplements and 5% (v/v) fetal bovine serum (FBS) and maintained at 37°C in a humidified normoxia condition (21% O_2, 5% CO_2, 74% N_2) or hypoxia condition (3% O_2, 5% CO_2, 92% N_2). Cells were passaged (passages 4–6) after reaching 80–90% confluence, detached with 0.05% trypsin, 0.04% EDTA (Sigma-Aldrich, MO, USA, Cat.No.EDS-100G) in phosphate-buffered saline (PBS). In this study, PAECs were treated with

TRAF6 inhibitor (C25-140, 10 μM, MCE, USA, Cat.No.HY-120934) , NF-κB inhibitor (JSH-23, 30 μM, MCE, USA, Cat.No.HY-13982) , Cul 5 NEDDylation inhibitor (Pevonedistat, 0.5 μM, MCE, USA, Cat.No.HY-70062).

The experimental animals were approved by the Institutional Animal Care and Use Committee of Capital Medical University and Xi'an Jiaotong University. Animals were housed in accordance with the regulations for the Management of Laboratory Animals published by the Ministry of Science and Technology of the People's Republic of China. Eight-week-old male C57BL/6 mice weighing 20–25 g were bought from Vital River Laboratory Animal Technology Company (Beijing, China). Mice were exposed to normobaric hypoxia (10% O_2) in an airtight plexiglass chamber for 4 weeks. Control mice were exposed to room air under the same conditions.

Lung tissue samples preparation

The study was approved by the Research Ethics Committee of Capital Medical University and Xi'an Jiaotong University. Written informed consent was obtained from all patients before the procedure. The lung tissues were obtained via lung transplantation or lobectomy both from bronchiectasis/bronchiectasis-PH patients and donors, and fixed in the 10% of formaldehyde, then embedded in paraffin. The patients' clinical data can be seen in our previous published paper[14] and in the Table S1.

METHOD DETAILS

Cell samples and RNA preparation

Cell growth was arrested by incubating in 2% serum and GS-free ECM for 6 h under normoxia, then growth-arrested cells were incubated with low-serum (5% FBS) and GS-free ECM under normoxia or hypoxia for 24 h (n = 3 for each group). Total RNA was isolated with TRIzol reagent (Invitrogen, USA, Cat.No.15596-026) and purified using RNeasy Mini Kit (Qiagen, German, Cat.No.74106), including a DNase digestion treatment. RNA concentrations were determined by the absorbance at 260 nm and quality control standards were A260/A280 = 1.8–2.1, using NanoDrop 2000 (Thermo, America).

Microarray processing

cDNAs of samples from normoxia and hypoxia group were hybridized to Affymetrix Clariom D human GeneChip arrays (Affymetrix, America) according to the User Manuals. Affymetrix Expression Console Software (version 1.2.1) was used for microarray analysis. Raw data (CEL files) were normalized at transcript level using robust multiaverage method (RMA workflow). Median summarization of transcript expressions was calculated. Gene-level data were then filtered to include only those probe sets that are in the 'core' metaprobe list, which represent RefSeq genes.

Global Signal Transduction Network

To detect the over-representation of pathways involved among the large list of genes from High-throughput experiments such as microarray and NGS, which is known as an effective way to hunt the downstream targets. The hypergeometric distribution was used to calculate the pathway enrichment, and fdr was used to adjust the p values for multiple comparisons. After parsing the whole KEGG database, all study genes involved pathways were extracted, and the study pathway network was generated with the help of the pathway topology in the KEGG database. The specific gene network of one pathway was generated based on the pathway topology analysis, and the study gene network was generated after mapping to the generated reference KEGG gene network (i.e., a collection of gene networks from each pathway).

Adeno-associated virus vector delivery

HBAAV2/VEC-TIE-mir30-*m*-CUL5 shRNA-ZsGreen vector and HBAAV2/VEC-TIE-ZsGreen control vector were purchased from Hanbio Tech (Shanghai, China). The genomic titer was $1.7–1.8\times10^{12}$ genomic copies per mL determined by quantitative PCR. For delivering AAV vector, male C57BL6/mice (8 weeks of age) were administered as previously described.[39] AAV vectors were administered in a volume of 100 μL with a titer of 1×10^{11} viral genome copies of warm sterile saline via intratracheal injection followed by anesthesia. After the treatment, mice were placed on a warm pad until they woke up. Then the model of hypoxia-induced PH began to be generated.

Immunohistochemical analysis

Cul 5 expression levels were detected in paraffin-embedded lung tissue sections using anti- Cul 5 (Abcam, UK, 1:100 dilution, Cat.-No.ab264284) antibody. Protein expression was visualized using HRP-conjugated secondary antibody (R&D, CA, USA, 1:200 dilution, Cat.No.HAF017). The positive cells were developed by diaminobenzidine (DAB) reagent, nuclei were counterstained with hematoxylin.

Immunofluorescent analysis

Cul5 expression levels were detected in paraffin-embedded lung tissue sections using the anti-Cul5 antibody (Abcam, UK, 1:200 dilution, Cat.No.ab264284), CD31 antibody (Abcam, UK, 1:200 dilution, Cat.No.ab182981) protein expression was visualized using Alex Fluor 488 and Alex Fluor 594 secondary antibodies (ZSGB-BIO, China, 1:200 dilution, Cat.No.ZF0511,ZF0516). Nuclei were counterstained with DAPI.

Tubule formation assay

To detect the human PAECs tube formation ability, a tube formation assay was performed. BD matrigel (BD Biosciences, USA, Cat.No.356234) was distributed in a 24-well plate (200 μL/well) on ice and allowed to solidify at 37°C for at least 30 min. After the matrigel mixture solidified, human PAECs (1×10^5 per well) were gently added to each of the triplicate wells. Tube formation was quantitatively measured by calculating the total tube length and tube number of tube-like structures using the NIS-Elements Basic Research-Microscope Imaging Software (Nikon, Tokyo, Japan). Tracks of endothelial cells that were organized into networks of cellular cords were counted in 6 random fields.

Cell adhesion assay

Cells were trypsinized and seeded on top of fibronectin (30 μL 20 μg/mL; MILLIPORE, USA, Cat.No.FC010)-coated 96-well plate (1×10^4 per well in 5% FBS and growth factor–free ECM) and incubated for 30 min at 37°C. After washed with PBS, the adhesion cells were photographed (4 pictures per well, 5 wells for one group) and data were analyzed by ImageJ software.

Plasmid construction

Cul 5 overexpression plasmid was constructed. In brief, specific primers used to amplify the coding region of H-VACM-1 (Cul-5) were Cul 5-Forward: 5′-TGAGAAGGCATACTTGGAT-3′ and Cul 5-Reverse: 5′-AACGGAGTTACATTCTCGTCTTG-3′. The above PCR products (length 169 bp) were subcloned into pcDNA3.1-3xFlag-Puro vector. The inserts were inserted into the Xholand Hind III sites of the vector, plasmids containing the insert were isolated for sequencing.

Cell transfection

Cells were cultured at 50% confluence. Transient transfection of siRNA of VEGF was carried out using Lipofectamine 2000 reagent following the manufacturer's procedure. Briefly, PAECs were washed with serum-free medium and cultured in serum-free medium without antibiotics. The transfection complex (siRNA/plasmids and the transfection reagent mixture) was added to the medium in a drop-wise manner and mixed gently by rocking the media back and forth. After 4–6 h, the cell culture medium was changed back to ECM containing serum and antibiotics and incubated at 37°C for 48 h before subsequent experiments.

The sequences of siRNA were as follows:

Cul 5: sense: 5′ -GGCUAAUAGAGCACAAAUATT-3′
anti-sense: 5′ -UAUUUGUGCUCUAUUAGCCCTT-3′
NEDD8: sense: 5′ -GAGAAGACAGCAGCUGAUUTT-3′
anti-sense: 5′ -AAUCAGCUGCUGUCUUCUCTT-3′
VEGFA: sense: 5′ -GGCAGCUUGAGUUAAACGATT-3′
anti-sense: 5′ -UCGUUUAACUCAAGCUGCCTT -3′
Negative control (NC): sense: 5′ -UUCUCCGAACGUGUCACGUTT-3′
anti-sense: 5′ -ACGUGACACGUUCGGAGAATT-3.

Measurement of right ventricular systolic pressure

Mice were anesthetized with 2% pentobarbital (50 mg/kg, i.p.). Right ventricular systolic pressure (RVSP) was used as an indicator for the mean pulmonary arterial pressure. Our lab usually used the method of closed-chest insertion into the right ventricle (RV) to measure the RVSP.[40] A 22-gauge needle connected to a pressure transducer, which was interfaced with the PowerLab system (AD Instruments, Sydney, Australia), was inserted into RV of anesthetized animals through a xiphocostal angle approach, the waveform was used to confirm the position of the needle. Data were recorded using the Chart program, which was included with the PowerLab system. The mice were then sacrificed, and the hearts and lungs were collected.

Lung tissue preparation and morphometric analysis

Embedded in paraffin were serially sectioned at a thickness of 4 μm for standard H&E staining, immunohistochemistry and immunofluorescence. Pulmonary vessels with external diameters smaller than 100 μm were selected. Medial thickness was counted as follows: percent medial thickness (%MT) = $(\text{circumference}_{ext}/\pi - \text{circumference}_{int}/\pi)/(\text{circumference}_{ext}/\pi) \times 100$, and medial area = $\text{circumference}_{ext}^2/4\pi - \text{circumference}_{int}^2/4\pi$. The $\text{circumference}_{ext}$ and $\text{circumference}_{int}$ were demarcated by the external and internal elastic lamina. Images of pulmonary vessels were captured with Nikon microscope digital camera system and circumferences were measured with its image analysis program.

Measurement of right ventricular hypertrophy

Heart tissue was removed. The RV free wall was dissected from the left ventricle (LV) and ventricular septum (S). RV hypertrophy index (RVHI) was calculated by the wet weight ratio of RV to the LV plus S as the formula: $RV/(LV + S)\times100\%$. The ratio of RV weight to body weight (BW) was also examined. For wheat germ agglutinin (WGA) staining, slides were incubated for 30 min with 5 μM WGA dying (Invitrogen, USA, Cat.No.W11262) in the dark. The cell nuclei were stained with DAPI (ZSGB-BIO, China, Cat.No.ZLI-9557). The slides were sealed with antifade mounting medium and then observed using a fluorescence microscope.

Echocardiography

Echocardiography was performed using the Vevo 2100 high-resolution imaging system (FUJIFILM VisualSonics, Toronto, Canada) equipped with an 18- to 38-MHz (MS400, mouse cardiovascular) scan head. Transthoracic echocardiography was performed to measure pulmonary valve peak velocity (PV-peak), RV free wall thickness (RVWT), and tricuspid annular plane systolic excursion (TAPSE) as previously described in our published paper.[41] In brief, we used M-mode from the right parasternal short axis view to measure the right ventricle parameters at the end of a diastole. To determine TAPSE, the M-mode cursor was oriented to the junction of the tricuspid valve plane and the RV free wall using the apical four-chamber view. The peak velocity of the blood flowing through the pulmonary valve (PV) is determined at the tips of the pulmonic valve cusps.

Western blot

Lung homogenates were separated by SDS-PAGE and transferred to nitrocellulose membranes. Membranes were blocked in 5% non-fat dry milk for 1 h, followed by incubation in anti-Cul 5 (rabbit, Abcam, Cambridge, UK, 1:2000 dilution, Cat.No.ab184177), anti-TRAF6 (rabbit, Abcam, Cambridge, UK, 1:2000 dilution, Cat.No.Ab33915), anti-NF-κb (rabbit, Cell Signaling Technology, MA, USA, 1:1000 dilution, Cat.No.8242), anti-VEGF (rabbit, Affinity Biosciences, OH, USA, 1:1000 dilution, Cat.No.Af5131), anti-p-NF-κb(rabbit, Affinity Biosciences, OH, USA, 1:1000 dilution, Cat.No. AF2006), anti-HIF1 alpha (mouse, Affinity Biosciences, OH, USA, 1:1000 dilution, Cat.No.BF8002), anti-GAPDH (rabbit, Goodhere Biological Technology, Hangzhou, China, 1:1000 dilution, Cat.No.AB-P-R001) and anti-β-actin (mouse, proteintech, USA, 1 : 5000 dilution, Cat.No. 66009-1-Ig) antibodies overnight at 4°C. After the overnight incubation, membranes were washed with TBST buffer and re-incubated with a goat anti-rabbit IgG-HRP secondary antibody. The membranes were washed with TBST buffer and reacted with the electrochemiluminescence (ECL) substrate (Thermo, MA, USA, Cat.No.34579) and exposed to X-ray film. The value of the relative density of each target protein band was normalized to the density of the corresponding GAPDH band.

Immunoprecipitation (IP)

Total protein from cells was prepared using IP lysis buffer (abiowell, Hunan, China, Cat.No.AWB0164a) containing the protease inhibitor mixture. After quantification, proteins were immunoprecipitated with Cul 5 or TRAF6 primary antibody conjugated to protein G PLUS-Agarose beads (Santa, Texas, USA, Cat.No.sc-2003). The beads-proteins-antibody mixtures were washed three times with IP lysis buffer and the immunoprecipitated proteins were eluted by 16 SDS sample loading buffer (abiowell, Hunan, China, Cat.No.AWB0055), separated on 10% SDS-polyacrylamide gel, transferred onto nitrocellulose membrane. Immunostaining was performed using Western blot analysis as described above. TRAF6 was detected using anti-TRAF6 antibody (1:200, Santa Cruz, Texas, USA, Cat.No.sc-8409), and Cul 5 was detected using anti-Cul 5 antibody ((1:1000, Santa Cruz, Texas, USA, Cat.No.sc-373822). Ubiquitinated TRAF6 was detected using anti-ubiquitin antibody (1:1000, Proteintech, Des Plaines, USA, Cat.No.10201-2-AP), anti- TRAF6 antibody (1:200, Santa Cruz, Texas, USA, Cat.No.sc-8409), and anti-Rabbit/mouse IgG. Bands were visualized with chemiluminescence as described above.

QUANTIFICATION AND STATISTICAL ANALYSIS

Statistical tests are performed using GraphPad Prism (version 9). Data were expressed as means ± SD. Unpaired Student's *t* test was used for comparisons between two groups. One-way ANOVA with the Newman–Keuls was used to evaluate differences between more than two groups. $p < 0.05$ was considered statistically significant.